ACS OMEGA

Open Access

http://pubs.acs.org/journal/acsodf

Article

Jute Stick-Derived Cellulose-Based Hydrogel: Synthesis, Characterization, and Methylene Blue Removal from Aqueous Solution

Md. Sabbir Ahmed, Md. Maniruzzaman,* Md. Rubel Al-Mamun, Mohammad Amdad Ali, Md. Mizanur Rahman Badal, Md. Abdul Aziz, Mohammad A. Jafar Mazumder, Abbas Saeed Hakeem, and Mohammad Abu Yousuf

Cite This: *ACS Omega* 2023, 8, 47856−47873

Read Online

ACCESS | Metrics & More | Article Recommendations

ABSTRACT: In this work, microcrystalline cellulose (MCC) was isolated from jute sticks and sodium carboxymethyl cellulose (Na-CMC) was synthesized from the isolated MCC. Na-CMC is an anionic derivative of microcrystalline cellulose. The microcrystalline cellulose-based hydrogel (MCCH) and Na-CMC-based hydrogel (Na-CMCH) were prepared by using epichlorohydrin (ECH) as a crosslinker by a chemical crosslinking method. The isolated MCC, synthesized Na-CMC, and corresponding hydrogels were characterized by Fourier transform infrared (FTIR), X-ray diffraction (XRD), scanning electronic microscopy (SEM), and energy dispersive spectroscopy (EDS) for functional groups, crystallinity, surface morphology, and composite elemental composition, respectively. Pseudo-first-order, pseudo-second-order, and Elovich models were used to investigate the adsorption kinetics. The pseudo-second-order one is favorable for both hydrogels. Freundlich, Langmuir, and Temkin adsorption isotherm models were investigated. MCCH follows the Freundlich model (R^2 = 0.9967), and Na-CMCH follows the Langmuir isotherm model (R^2 = 0.9974). The methylene blue (MB) dye adsorption capacities of ionic (Na-CMCH) and nonionic (MCCH) hydrogels in different contact times (up to 600 min), initial concentrations (10−50 ppm), and temperatures (298−318 K) were investigated and compared. The maximum adsorption capacity of MCCH and Na-CMCH was 23.73 and 196.46 mg/g, respectively, and the removal efficiency of MB was determined to be 26.93% for MCCH and 58.73% for Na-CMCH. The Na-CMCH efficiently removed the MB from aqueous solutions as well as spiked industrial wastewater. The Na-CMCH also remarkably efficiently reduced priority metal ions from an industrial effluent. An effort has been made to utilize inexpensive, readily available, and environmentally friendly waste materials (jute sticks) to synthesize valuable adsorbent materials.

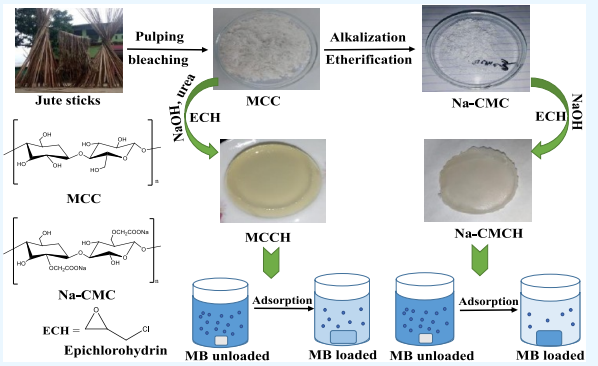

1. INTRODUCTION

In recent years, printing, textile, rubber, cosmetic, leather, plastic, food, and pharmaceutical processes have discharged dyes, pigments, and heavy metals.[1] Even a small quantity of dye emitted in wastewater has a significant environmental and ecological impact in addition to causing harm to human health.[2] Breathing issues, vomiting, diarrhea, and gastritis infections are related illnesses caused by methylene blue (MB).[3] It was thus necessary to develop an effective, low-cost, and ecological approach for removing such coloring contaminants and heavy metals from wastewater to safeguard the environment. Several methods have been explored to eliminate dye pollution from wastewater, including electrochemical treatment,[4] sonochemical treatment,[5] photocatalytic oxidation,[6] adsorption,[7] and sorbents.[8] Following the technique, adsorption technology appeared to be a more appealing and promising technique for dye removal due to its ease of recovery, simplicity, availability, efficiency, and ability to reuse the adsorbent.[9] The choice of adsorbent is critical for designing effective pollutant removal systems. The selectivity of an adsorbent for a specific pollutant depends on several factors, namely, chemical compatibility, surface properties, adsorbent−pollutant affinity, kinetics, and physical and chemical properties, of pollutants. Adsorbents select particular pollutants based on their chemical and biological properties and their specific

Received: August 25, 2023
Revised: November 15, 2023
Accepted: November 21, 2023
Published: December 11, 2023

Scheme 1. Preparation of MCC and Na-MCC (Step 1), MCC Hydrogel and Corresponding MB Removal (Step 2), and Na-CMC Hydrogel and Corresponding MB Removal (Step 3)

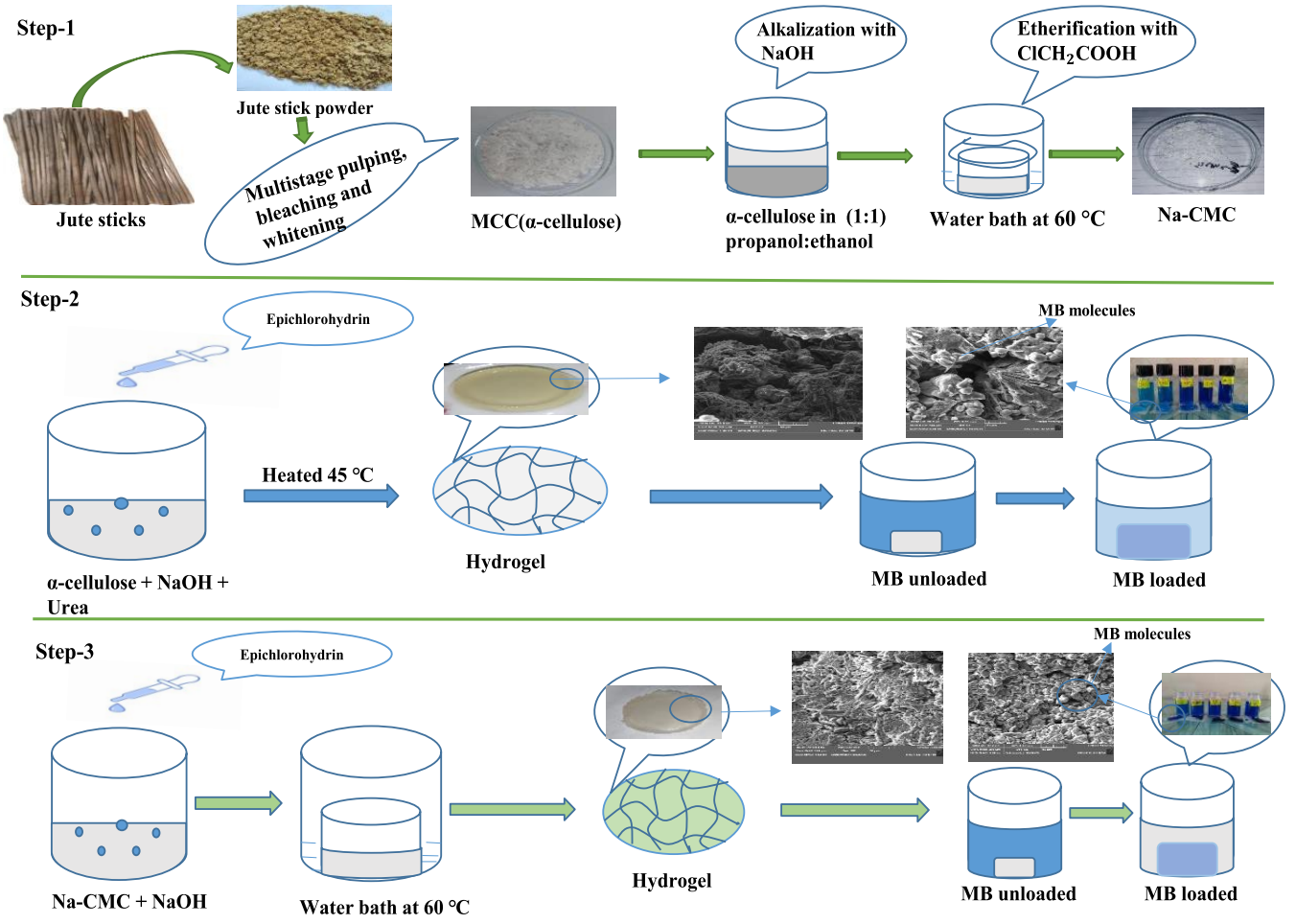

interactions at the adsorbent's surface. This work chose the hydrogel form of polymeric adsorbents obtained from natural sources that contained functional groups that are then easily chemically modified. These functional groups can capture the desired heavy metal ions and/or dyes. Due to their high selectivity to priority heavy metal ions, organic contaminants, and exceptional adsorption capability, these functionalities containing macromolecular structures as an adsorbent are of tremendous interest. Several synthetic polymeric adsorbents have recently been investigated to treat water-effluent wastes.[10−13] In particular, low-cost, ecofriendly, and biocompatible agents have attracted the most attention. Because of its high quality, cellulose is the most prevalent biopolymer on the planet and is renewable, biodegradable, and biocompatible.

Cellulose is a biodegradable and renewable polymer that is tough, fibrous, and water-insoluble and aids in maintaining the structure of the cell walls of plants and algae.[14−16] Cellulose has both crystalline and amorphous domains. According to the size and shape, there are two types of cellulose: microcrystalline cellulose and nanocrystal cellulose. The microcrystalline cellulose (MCC) material has the potential to be used in a variety of applications.[17−19] Efforts have been made to isolate the crystalline form of microcrystalline cellulose from raw materials such as bamboo, sugar beet pulp, cereal straw, etc.[20,21] Microcrystalline cellulose-based biocomposites are currently being investigated as a viable alternative to conventional polymeric composites.[22−24] It has some qualities such as cost effectiveness, high performance, durability, and fully sustainable technology to satisfy the consumer. These materials must be reliable, cheap, and economically viable and can show advanced performances and adaptable properties that can be used in the automotive, medical, building, and aerospace sectors.[25] It has great potential across several industries, such as food, cosmetics, medical, and pharmaceuticals. It can be employed in food as a binder and filler, as medicinal tablets, and most famously, as a reinforcing agent in constructing polymer composites.[26]

Wood, plants, and cotton linter are the most common and oldest raw materials used in MCC manufacturing.[27] In the past, researchers synthesized cellulose from different kinds of sources such as groundnut shells, cereal straw,[28,29] bamboo,[30] bagasse and corn cob,[31] sugar beet pulp,[32] luffa cylindrical,[33] olive stones,[34] jute,[35] rice and bean hulls,[36] newsprint,[37] hemp stalks and rice husks,[38] oil palm biomass,[39] wastepaper,[40] soybean hulls,[41] filter paper,[42] and cotton waste,[43] which have been investigated as significant resources of MCC. Researchers are now more interested in looking for alternate resources to produce cellulose. In this work, cellulose was synthesized from jute sticks as they are a readily available and abundant agricultural waste in Bangladesh and India. In Bangladesh, jute (*Corchorus capsularis*) is recognized as a golden fiber. These sticks were sold in the local market as fuel after fiber collection. The utilization of jute sticks as cooking fuel decreases daily for the development of gas stoves, electric stoves, etc.[44]

https://doi.org/10.1021/acsomega.3c06349
ACS Omega 2023, 8, 47856−47873

Bangladesh receives 3−4 million tons of jute sticks annually as agricultural trash.[45] The jute stick contains 40.8−47.5% α-cellulose, 23−23.6% hemicelluloses, 22.3−23.5% lignin, 3.6−4.7% acetyl content, 0.5−0.7% pectin, 0.6−0.8% ash, and 1.7−2.4% fats and waxes.[46] It was found that jute sticks are the most abundant sources of cellulose (40.8−47.5%). Therefore, it can be a suitable raw material to synthesize cellulose. The MCC market demand is expected to reach 1214.4 million US$ by 2023, increasing at a CAGR (compound annual growth rate) of 7%.[47] Thus, agricultural waste such as jute sticks can be used as a valuable commodity. To the best of our knowledge, this is the first study reporting on synthesizing α-cellulose from jute sticks and its application in a hydrogel as an adsorbent for removing MB from an aqueous solution.

Na-carboxymethyl cellulose (Na-CMC) is a water-soluble, anionic cellulose derivative and a linear polymer containing anhydro-glucose.[14] Cellulose has different kinds of nonionic and anionic derivatives such as ethyl cellulose (EC), hydroxy ethyl cellulose (HEC), hydroxy propyl cellulose (HPC), methylcellulose (MC), hydroxy propyl methylcellulose (HPMC), and anionic ether derivatives such as sodium-carboxy methylcellulose (Na-CMC).[14] These nonionic and ionic cellulose types can be used to prepare anionic and nonionic hydrogels. Hydrogels are insoluble, three-dimensional (3D), hydrophilic polymers that are mechanically or chemically crosslinked.[48] Hydrogels are primarily made from a combination of cellulose and a crosslinker. In this work, MCC- and Na-CMC-based hydrogels were prepared by a crosslinking method, where epichlorohydrin was used as a crosslinker. It has numerous applications in the food industry, cosmetic industry, drug delivery system, wound dressing,[49] and superadsorbents for the removal of dyes and heavy metals from wastewater.

This work aims to prepare and characterize cellulose (α-cellulose and Na-CMC)-based nonionic and ionic hydrogels from agricultural waste such as jute sticks. The synthesized nonionic (MCCH) and ionic (Na-CMCH) hydrogel was explored to remove MB from the aqueous solution. The swelling ratio was determined for both types of hydrogels. The effects of the temperatures, contact time, and dye concentration on the MB dye adsorption characteristics were determined. Several kinetic and isotherm models also investigated the adsorption behavior, such as kinetics and isotherms. Importantly, this work explores the effectiveness of a cellulose-based nonionic and ionic hydrogel on adsorption to remove the MB dye and the mechanism underlying the adsorption process.

2. MATERIALS AND METHODS

2.1. Materials. Jute sticks were collected from the local market of the Khulna division of Bangladesh. Toluene (99.2% purity), ethanol, sodium hydroxide (analytical grade), nitric acid (69% purity), sodium nitrite (99.2% purity), and acetic acid (99.85% purity) were purchased from Sigma-Aldrich and used as received. Sodium sulfite, sodium hypochlorite (6%), and propanol were purchased from Merck Science Private Limited. Monochloroacetic acid, methanol, epichlorohydrin, urea, and methylene blue were purchased from Research Laboratory Fine Chem Industries.

2.2. Preparation of MCC (α-Cellulose). The isolation method of MCC from the jute stick was followed by Suryadi et al. with slight modification[50] (step 1 of Scheme 1). Briefly, jute sticks were cleaned with water and dried at 60 °C for 24 h. The cleaned jute sticks were crushed, milled into fine powder, and screened through a 1.18 mm sieve. The jute stick powder was then defatted by elution with toluene/ethanol (2:1 v/v) three times using a hot extractor at 45 °C for 6 h. It was then air-dried and treated with 10% (w/v) sodium hydroxide at 55 °C for 90 min. After that, the residue was neutralized with acetic acid, rinsed with cold water, dried in a convection oven at 80 ± 5 °C for 5 h, and stored in a closed container. To remove lignin, 30 g of jute stick powder and 4 mg of sodium nitrite were added to 400 mL of 3.5% nitric acid and treated for 2 h at 90 °C with constant stirring. It was then digested for 1 h at 50 °C in 2% (w/v) sodium hydroxide and sodium sulfite. The precipitate was filtered and washed with distilled water. It was then bleached with 3.5 wt % sodium hypochlorite at 90 °C for 10 min. The residue was washed with water and treated with 17.5% (w/v) sodium hydroxide for 30 min at 80 °C. The resultant α-cellulose was filtered and washed thoroughly with distilled water. For whitening the α-cellulose, it was treated with 3.5% (w/v) sodium hypochlorite for 5 min at 100 °C. The bleached cellulose product was washed, filtered, and carefully squeezed out of the water to make little lumps. It was then dried to a constant weight in a convection oven drier at 60 °C. The MCC yield from jute sticks was determined to be ≈40%.

2.3. Preparation of Na-Carboxymethyl Cellulose (Na-CMC). To synthesize Na-CMC from isolated α-cellulose, the method of Hong et al. was used with slight modification[51] (step 1 of Scheme 1). 2 g of α-cellulose powder was added to a 60 mL binary mixture of isopropyl alcohol (50%) and ethanol (50%). A 1.6 g portion of 25% (w/v) sodium hydroxide was added to the mixture with constant stirring for 1 h. After that, 2.4 g of monochloroacetic acid was added to the mixture, thus creating carboxy functional groups. The mixture was covered with aluminum foil and set in a water bath for 3 h at 70 °C with constant stirring. The slurry was then immersed in 22.5 mL of methanol and neutralized with acetic acid (90%). The resultant product was rinsed five times with 70% ethanol followed by methanol to eliminate impurities. It was then dried in a convection oven drier at 45 °C. Finally, 96.3% Na-CMC was obtained from MCC.

2.4. Preparation of the MCC Hydrogel (Nonionic Hydrogel). The method of Qin et al. was slightly modified to prepare MCCH[52] (step 2 of Scheme 1). Briefly, 3 g of NaOH and 2 g of urea were dissolved in 50 mL of distilled water. Then, 1 g of cellulose was added to this mixture, stirred for 5 min, and stored in a refrigerator at −5 °C for 12 h. The frozen solid was thawed and stirred at room temperature, thus becoming a colorless clear cellulose solution. 4.5 mL of ECH was then dropped into the cellulose solution and stirred for 1 h at 25 °C. The mixture was heated at 50 °C without stirring for 20 h. The resultant cellulose hydrogel was washed vigorously with water to remove the unreacted species. The obtained hydrogel was vacuum-dried and stored in a refrigerator at 10 °C for further use.

2.5. Preparation of the Na-CMC Hydrogel (Anionic Hydrogel). The slightly modified method of Yadollahi et al. was used to prepare Na-CMCH[53] (step 3 of Scheme 1). A 1.5 g portion of Na-CMC was dissolved in 50 mL of 3% w/v NaOH solution and stirred continuously for 2 h. After that, 3 mL of epichlorohydrin was added dropwise with constant stirring. The mixture was then heated to 60 °C in a water bath for 2 h. The crosslinked Na-CMC paste was then collected and

https://doi.org/10.1021/acsomega.3c06349
ACS Omega 2023, 8, 47856−47873

washed multiple times with distilled water, dried for 24 h in a convection oven at 45 °C, and stored at room temperature.

3. CHARACTERIZATION

3.1. Lignin Test of Microcrystalline Cellulose. Small amounts of the delignified sample (A) and lignin-containing sample (B) were taken in different test tubes, immersed in 1% potassium permanganate ($KMnO_4$), and kept for 5 min. Then, the $KMnO_4$ was decanted from the sample twice. After that, the sample was treated with 3% HCl solution until the color turned black or dark brown to light brown. The resultant light-brown sample was again immersed in HCl solution and washed twice. The sample was then treated with conc. NH_4OH. No color change occurred for the delignified sample (A), and a red color was developed for lignin-containing sample (B) (Figure 1).

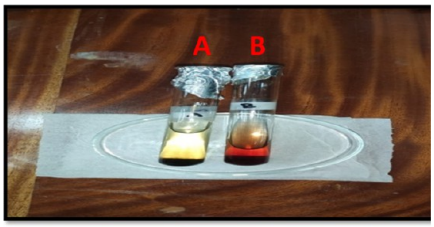

Figure 1. Lignin test result.

3.2. Fourier Transform Infrared Spectroscopy (FTIR). A Thermo Nicolette iS50 FTIR spectrometer (spectral resolution: 4 cm^{-1}; number of scans: 16) was used to record spectra.

3.3. Degree of Swelling. The MCCH and Na-CMCH hydrogels were cut and immersed in distilled water for 24 h at 25 °C. After the time had elapsed, the swollen hydrogel was gently removed, and excess surface water was removed using tissue paper. The swollen hydrogel was weighed, and the degree of swelling was estimated using eq 1

$$\text{degree of swelling}\ (\%) = (W_t - W_d)/W_d \times 100 \quad (1)$$

where W_t and W_d refer to the weight of the swollen hydrogel and initial dry hydrogel, respectively.

3.4. X-ray Diffraction (XRD). A high-resolution X-ray diffractometer (Bruker D8 Advanced XRD system) was used to examine the crystalline structure of the MCC, Na-CMC, and hydrogels. The crystallinity of MCC and Na-CMC was investigated from X-ray diffraction curves following the Segal Method in Kunusa et al.[31]

The crystallinity index (CrI) of MCC and Na-CMC was determined according to eq 2

$$\text{CrI}\ (\%) = (I_{002} - I_{Am})/I_{002} \times 100 \quad (2)$$

where I_{002} refers to the peak intensity of the crystallite domain and I_{Am} refers to the peak intensity of the amorphous domain.

3.5. Surface Morphology. *3.5.1. Scanning Electronic Microscopy (SEM).* The surface morphology of MCC, Na-CMC, and corresponding hydrogels and the cross-sectional morphology of the hydrogel were determined using FESEM (TESCAN-LYRA-3, Czech Republic).

3.5.2. Energy Dispersive Spectroscopy (EDS). The FESEM -EDS spectrometer-equipped Oxford instrument Xmass detector with a filament voltage of 10 keV determined the element content of MCC, Na-CMC, and hydrogels.

3.6. Adsorption Studies. To determine adsorption experiments, 0.4 g of hydrogels was mixed with (10, 20, 30, 40, and 50 mg/L) 40 mL of dye (MB) solutions separately with appropriate concentration and temperature. The different dye concentrations before and after the adsorption were measured by using a UV-1800 Shimadzu UV spectrophotometer.

The adsorption capacity and percentage of dye removal efficiency of the hydrogel were estimated using eqs 3 and 4, respectively

$$\text{adsorption capacity, } q_e = [(C_0 - C_e)/m] \times v \quad (3)$$

$$\text{removal efficiency, } \% = [(C_0 - C_e)/C_0] \times 100 \quad (4)$$

where C_0 is the initial concentration and C_e is the equilibrium concentration of the dye solutions; q_e (mg/g) refers to the adsorption capacity of the hydrogel; V is the volume of the solution (mL); and m refers to the mass of the hydrogel (g).

3.7. Adsorption Kinetics. The adsorption kinetics of both types of hydrogels were determined by fitting the adsorption kinetics on various concentrations of MB dye solution with pseudo-first-order (eq 5), pseudo-second-order (eq 6), and Elovich (eq 7) kinetic models.

$$\ln(q_e - q_t) = \ln q_e - k_1 t \quad (5)$$

$$\frac{t}{q_t} = \frac{t}{q_e} + \frac{1}{k_2 q_e^2} \quad (6)$$

$$q_t = \frac{1}{\beta}\ln(\alpha\beta) + \frac{1}{\beta}\ln t \quad (7)$$

where q_e (mg/g) refers to the equilibrium adsorption capacity of the hydrogel, q_t (mg/g) refers to the adsorption capacity of the hydrogel at a particular time, k_1 and k_2 are one- and two-stage adsorption rate constants, respectively, t is the adsorption time (min), α (mg min/g) refers to the initial adsorption rate constant, and β (g/mg) is a factor associated with the extent of surface coverage and activation energy for chemisorption.

3.8. Adsorption Isotherms. At equilibrium, the Langmuir and Freundlich models are employed to characterize the interaction between the hydrogel and dye. Equations 7, 8, and 9 represented the Langmuir, Freundlich, and Temkin models, respectively.

$$\frac{1}{q_e} = \frac{1}{q_m} + \frac{1}{q_m k_L}\frac{1}{C_e} \quad (8)$$

$$\ln q_e = \ln K_F + \frac{1}{n}\ln C_e \quad (9)$$

$$q_e = B \ln A_T + B \ln C_e \quad (10)$$

where q_e (mg/g) refers to the equilibrium adsorption capacity of the hydrogel, q_m (mg/g) refers to the highest adsorption capacity of the hydrogel, C_e (mg/mL) is the equilibrium MB concentration, K_L (L/mg) is the affinity of adsorption active sites, K_F (L/mg) refers to the Freundlich isotherm constants related to adsorption capacity, n refers to the constant of adsorption intensity, B (J/mol) is the Temkin isotherm constant related to the heat adsorption, and A_T (L/g) is the Temkin constant.

3.9. Reusability Studies. The regeneration of an adsorbent plays an essential role in making the adsorption process cost-competitive and environmentally friendly. The

https://doi.org/10.1021/acsomega.3c06349
ACS Omega 2023, 8, 47856−47873

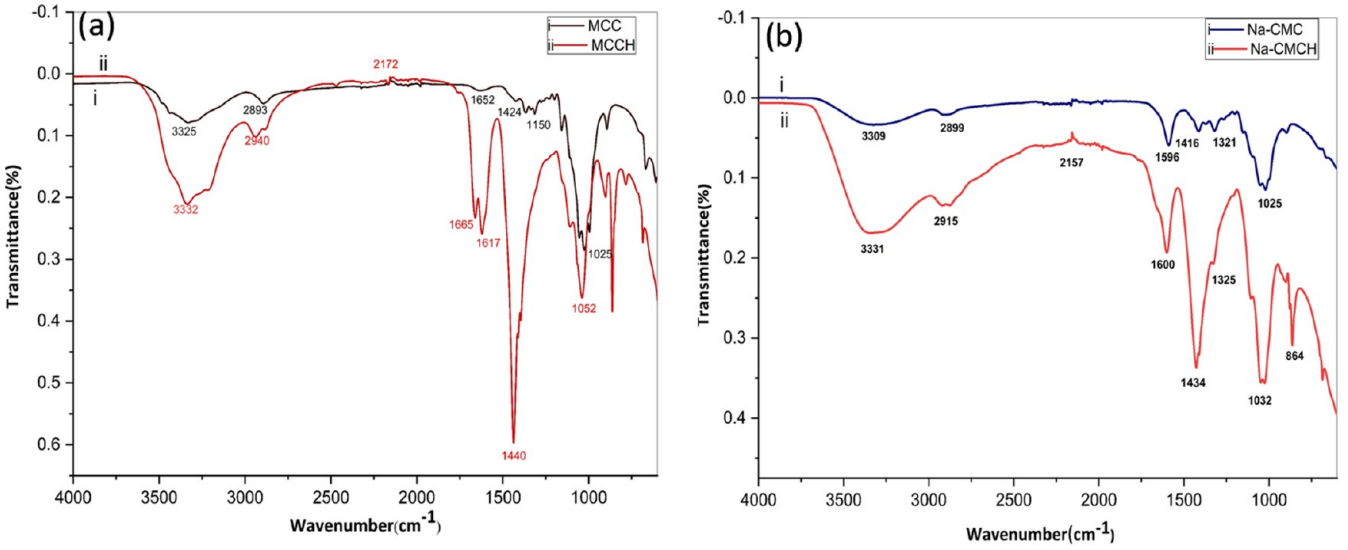

Figure 2. FTIR spectra of (a) MCC and MCCH and (b) Na-CMC and Na-CMCH.

Scheme 2. Reaction Scheme for the Preparation of MCCH and Na-CMCH

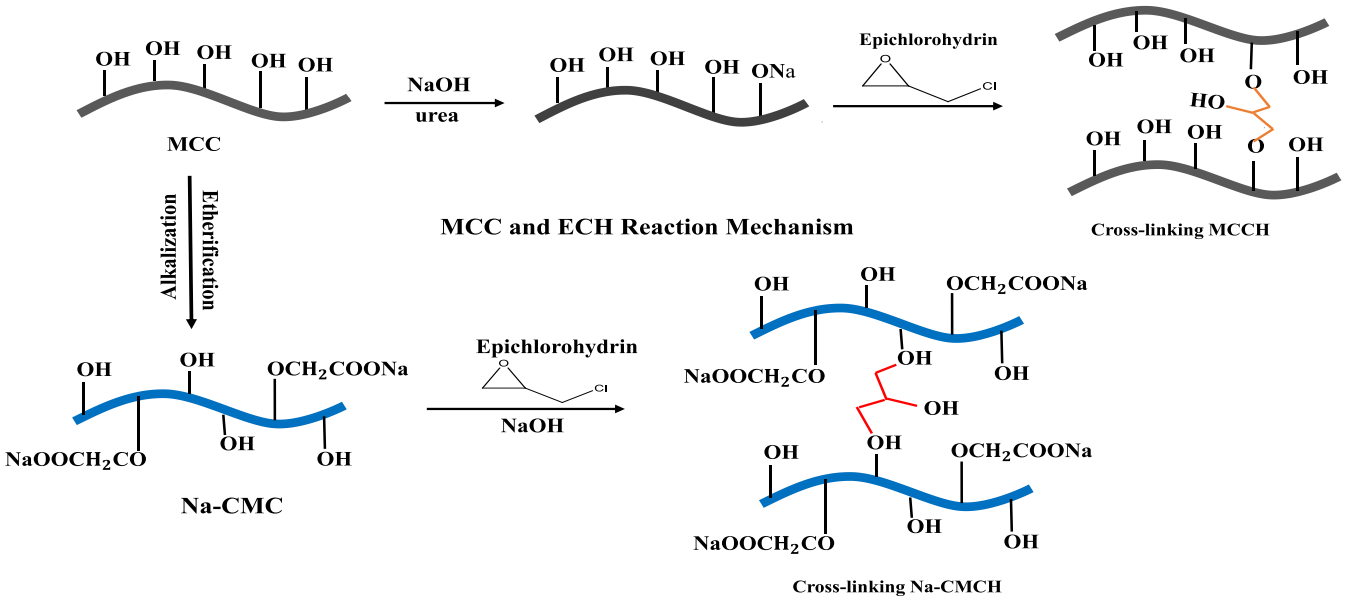

adsorption and desorption behaviors of both nonionic and anionic hydrogels was determined. The highest desorption of cationic dyes (MB) occurs in the acidic environment. The adsorption experiment was carried out at a constant temperature of 298 K with an incubator shaker set to 90 rpm. The initial dye concentration was 10 mg/L, and the adsorbent dosage was 0.2 g. After 6 h of stirring, the supernatant was analyzed by UV−vis spectroscopy to determine the concentration of MB in the solution. The desorption study was conducted in 10 mL of 0.1 M HCl for 30 min, followed by centrifugation and washing with 5 mL of water. The two supernatants were combined and analyzed to determine the desorbed MB. These methods were repeated three times to determine the adsorbent's reusability.

4. RESULTS AND DISCUSSION

4.1. FTIR. FTIR spectra of MCC, MCCH, Na-CMC, and Na-CMCH are shown in Figure 2. For MCC and MCCH (Figure 2a), the stretching of a significant number of hydroxyl groups on the cellulose and hydrogel structures was attributed to the wide absorption band at 3300−3500 cm^{-1}. The absorption band at 2893 cm^{-1} in the spectra of microcrystalline cellulose is due to C−H symmetric stretching, which had migrated to 2940 cm^{-1} in the hydrogel spectrum, indicating efficient crosslinking in the hydroxyl group of microcrystalline cellulose. The peak observed in the microcrystalline cellulose at 1652 cm^{-1} had moved to the higher wavenumber of 1665 cm^{-1} for the hydrogel, which was more intense. As a result, microcrystalline cellulose reacted with ECH to shift an apparent peak in the hydrogel spectrum. The observed peaks at about 1617 cm^{-1} in the spectra of hydrogels are attributed to the C═O stretching in the ester linkage that may give the

https://doi.org/10.1021/acsomega.3c06349
ACS Omega 2023, 8, 47856−47873

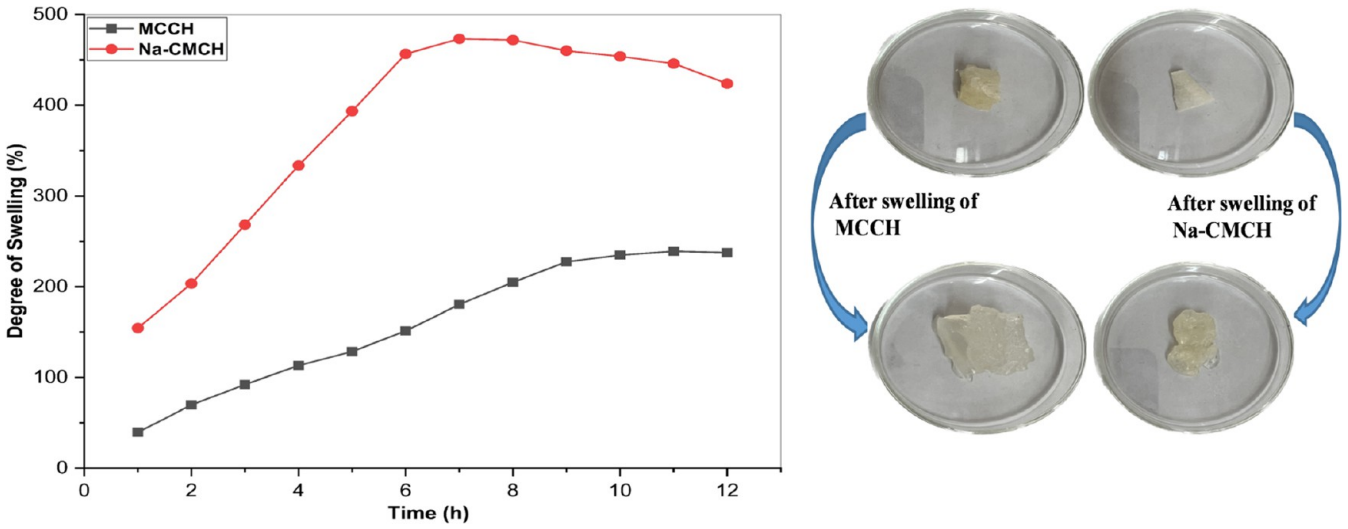

Figure 3. Swelling degrees of MCCH and Na-CMCH in distilled water at 25 °C.

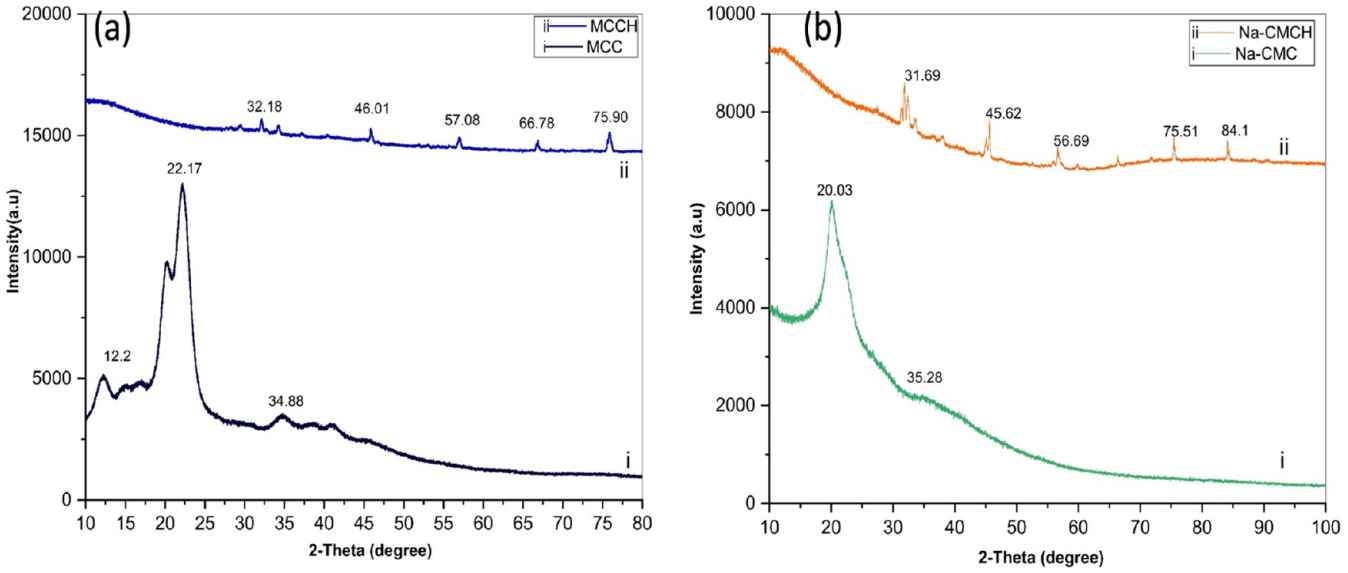

Figure 4. XRD spectrum of (a) MCC and MCCH and (b) Na-CMC and Na-CMCH.

surety that crosslinking has happened in the hydrogel.[54] The peak at 1440 cm^{-1} is due to the CH_2 bending vibration of the hydrogel. The probable reaction mechanisms of MCC and ECH are shown in Scheme 2. The characteristics of a glycosidic group of C−O, C−O−C, and C−OH bonds were seen in the spectrum of microcrystal cellulose at 1150 cm^{-1}. Stretching of C−O and C−C groups at 1025−1060 cm^{-1} aids in synthesizing alkali-cellulose. There are sharp peaks at 893 cm^{-1}, which is typical for the β-glycosidic linkage of cellulose. Figure 2b shows the FTIR spectra of Na-CMC and the Na-CMC-based hydrogel. The functional groups seen in the infrared spectra of carboxymethyl cellulose are as follows: OH group at a wavenumber of 3650−3200 cm^{-1}, C−H stretching at 3050−2950 cm^{-1}, CH_2 at 1416 cm^{-1}, C−OH bond at 990−1250 cm^{-1}, and C−O−C glycosidic at 1200−980 cm^{-1}. Carboxyl groups and their salts exhibit two peaks at 1590−1650 and 1410−1460 cm^{-1}, indicating the existence of a carboxymethyl substituent. The CH_2 scissoring and OH bending vibration are ascribed to the band at about 1410−1440 and 1321 cm^{-1}, respectively.[55]

The distinctive absorption peaks at 3331 and 2915 cm^{-1} due to the crosslinked hydrogel correspond to OH and CH stretching of vibrations, respectively. Almost identical peaks were observed for Na-CMC and Na-CMCH. The reaction mechanism of crosslinking Na-CMCH is shown in Scheme 2. A significant peak at 1325 cm^{-1} is shown in the crosslinking hydrogel, the effective ether-based crosslinking between Na-CMC and ECH (Figure 2b).

4.2. Degree of Swelling. Swelling properties of MCCH and Na-CMCH were determined in double-distilled water at 25 °C. The capacity to absorb water of the hydrogel significantly impacted the removal of the MB dye. In Figure 3, the maximum degree of swelling of the MCCH and Na-CMCH could reach about 239 and 473%, respectively; it was determined against the original dry weight of both hydrogels at 25 °C. Carboxylic groups of Na-CMC-based polymer networks are ionized above their pK_a value (about 4.3) in the pH domain. The same-charged chains repel each other, causing the polymer network to expand and the hydrogel to be swollen.[56] The chemical crosslinking of epoxy groups on ECH and

https://doi.org/10.1021/acsomega.3c06349
ACS Omega 2023, 8, 47856−47873

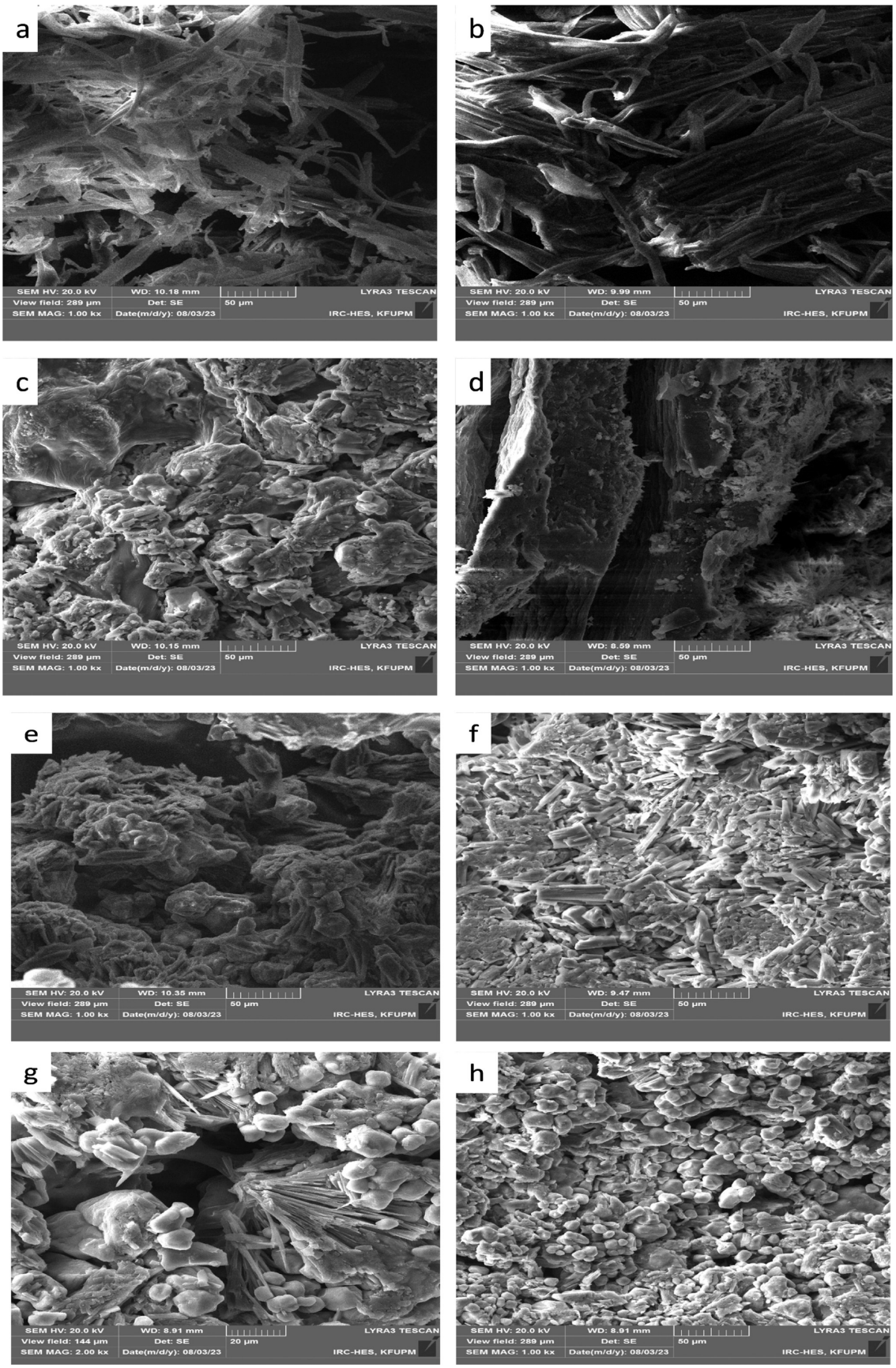

Figure 5. SEM images for the surface morphology of (a) MCC, (b) Na-CMC, (c) MCCH, and (d) Na-CMCH and cross-sectional morphology of (e) MCCH, (f) Na-CMCH, (g) MCCH with MB loaded, and (h) Na-CMCH with MB loaded.

https://doi.org/10.1021/acsomega.3c06349
ACS Omega 2023, 8, 47856−47873

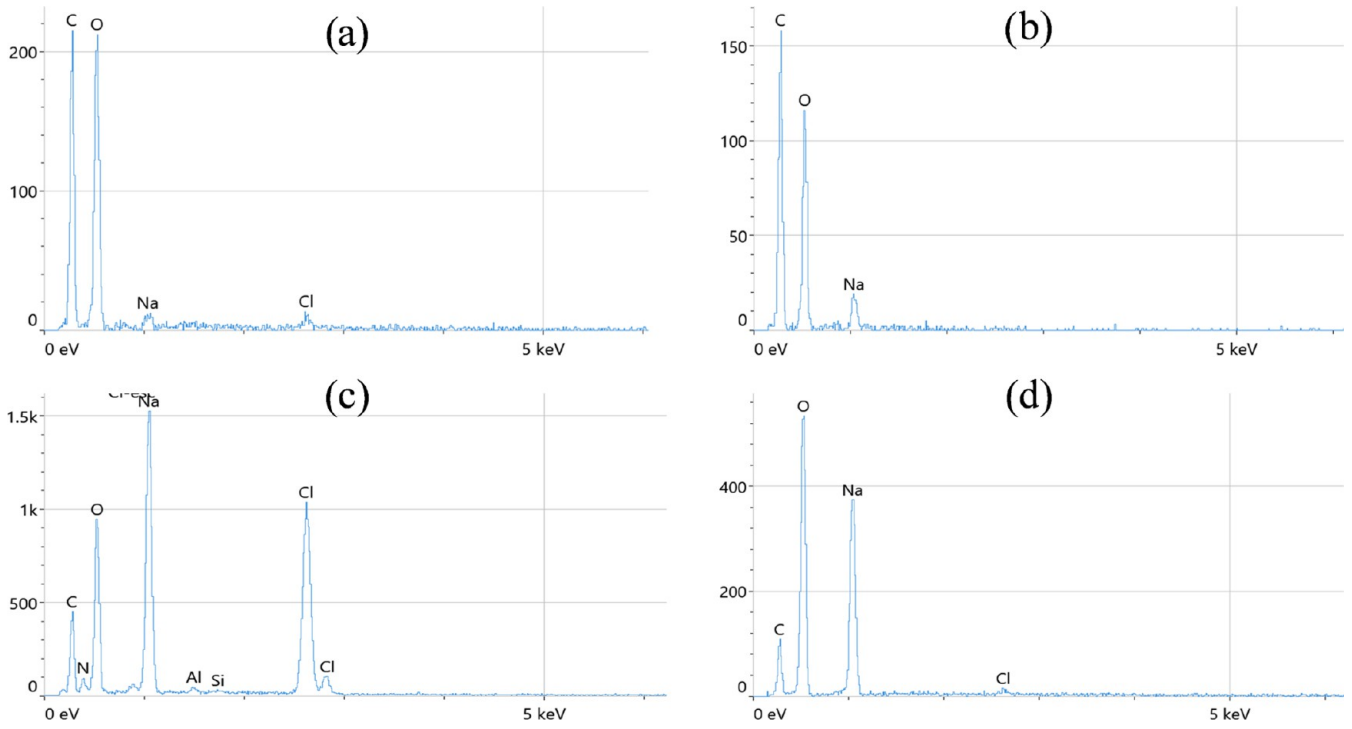

Figure 6. EDS analysis of (a) MCC, (b) Na-CMC, (c) MCCH, and (d) Na-CMCH.

hydroxyl groups on cellulose reduced the average distance between crosslinking sites.[54] As a result, the swelling degree of the cellulose-based hydrogels dropped. The great swelling capacity favored high-quantity dye transport inside the hydrogel as well as substantial exposure of active regions of hydrogels to dyes.[57]

4.3. XRD. The XRD spectra of the MCC and its hydrogel are presented in Figure 4a, which shows numerous sharp and distinguished peaks. The peaks of MCC were found at 2θ = 12.2, 22.17, and 34.85°, which refer to the crystallographic planes of 110, 200, and 004, respectively. The peaks at 12.2 and 22.7 are observed to be sharpened for MCC, but the sharp peaks could not be seen in the MCCH spectrum. The crystallinity index was recorded by the Segal equation (eq 2). The crystallinity index was recorded as 74% for MCC, whereas the XRD pattern of the MCC hydrogel showed numerous sharp and distinguished peaks observed at 2θ = 32.18, 46.01, 57.08, 66.78, and 75.90°. These peaks reflect the MCC−ECH hydrogel for the presence of ECH. When comparing the X-ray diffraction pattern of Na-CMC and its hydrogel, it is clear that all of the peaks of MCC disappeared, but the hydrogel showed an ECH crystalline structure that was almost amorphous.

The XRD pattern of the Na-CMC and its hydrogel is depicted in Figure 4b, which showed numerous sharp and distinguished peaks. The peaks of Na-CMC were found at 2θ = 20.03 and 35.28°. Na-CMC compounds can be identified as absorption of 2θ = 20°. This is in accordance with the results of the study of Suripto et al.,[55] which explained that the XRD CMC diffractogram was found at 2θ = 20°. In the current study, the Na-CMC diffractogram was also found at 20.03°.

In contrast, the XRD pattern of the hydrogel showed numerous sharp peaks observed at 2θ = 31.69, 45.62, 56.69, 75.51, and 84.1°. These peaks reflect the Na-CMC and ECH hydrogel for the presence of ECH. It is found that the crystallinity index of the Na-CMC was recorded as 29.6%. When comparing the X-ray diffraction pattern of Na-CMC and its hydrogel, it is clear that all the peaks of Na-CMC disappeared, but the hydrogel showed an ECH regular crystalline structure but was mainly amorphous.

4.4. SEM. In Figure 5, the morphology of the isolated MCC has been reported. All of the fibers are formed in the bundles. Several cross-interlocking points and junctions are visible in Figure 5a. MCC was a short and thin structure, indicating that lignin, hemicellulose, and other contaminants were eliminated during the isolation process. It was also demonstrated that MCC had individualized fibers with rod-like shapes. The alkaline and bleaching processes separate the plant's components into well-separated fibrous strands. The lengthy microfibrillar structure and high aspect ratio of MCC make it appropriate to manufacture high-tensile strength biocomposite products. As shown in Figure 5b, the Na-CMC SEM examination was utilized to identify the morphological alterations of cellulose compounds to Na-CMC. The SEM results in Figure 5a,b revealed a density difference between cellulose and Na-CMC compounds. Na-CMC compounds have a more tenuous morphology than that of cellulose compounds. This is congruent with the findings of Hong et al.,[51] who discovered that Na-CMC compounds had been methylated as a result of carboxymethyl groups replaced on cellulose molecules, causing the shape of Na-CMC to become insignificant and the distance between molecules is increased.

Figure 5c,d shows the surface morphologies of the MCCH and Na CMC hydrogels. The structure of the hydrogel is not smooth and is found to be very porous. The electrostatic repulsions caused by the ionic charge of the carboxylate anions (COO−) in the hydrogel have increased the space of the crosslinked hydrogel network, which means that the space of the crosslinked hydrogel network has grown. As shown in Figure 5c,d, the gels exhibit an open porous geometry with a pore size separated by sheet-like walls and ultrathin structures. The hydrogels have high porosity, allowing for quick bulk penetration, which would benefit absorbent applications.

https://doi.org/10.1021/acsomega.3c06349
ACS Omega 2023, 8, 47856−47873

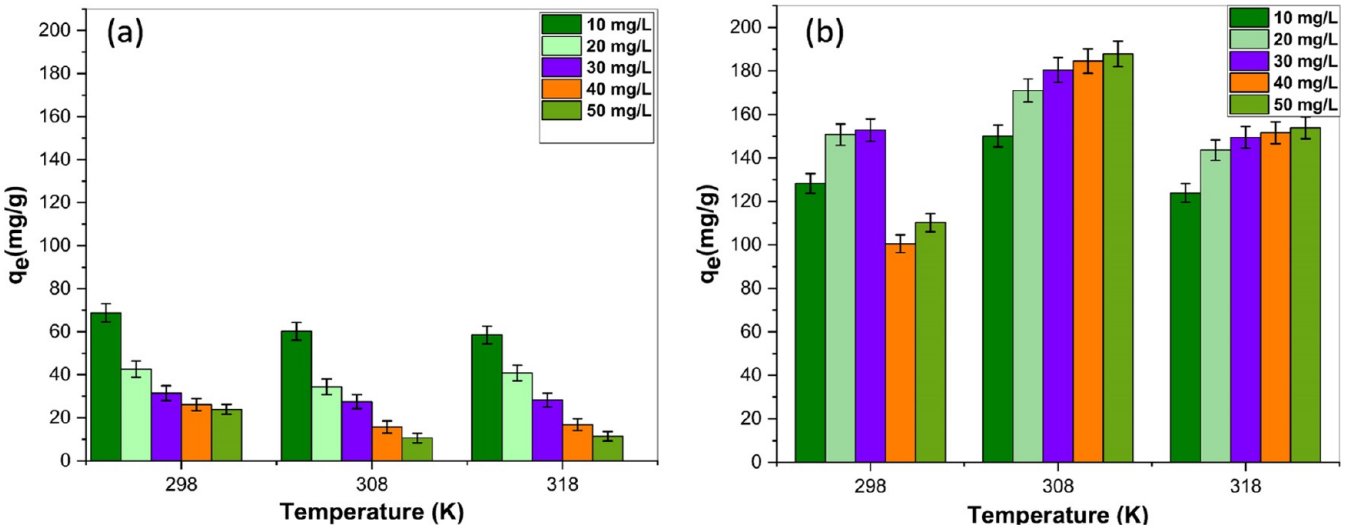

Figure 7. Temperature effect on dye adsorption (a) MCCH and (b) Na-CMCH (conditions: adsorbent dosage W_{Hg} = 0.3 g, V = 30 mL, in distilled water).

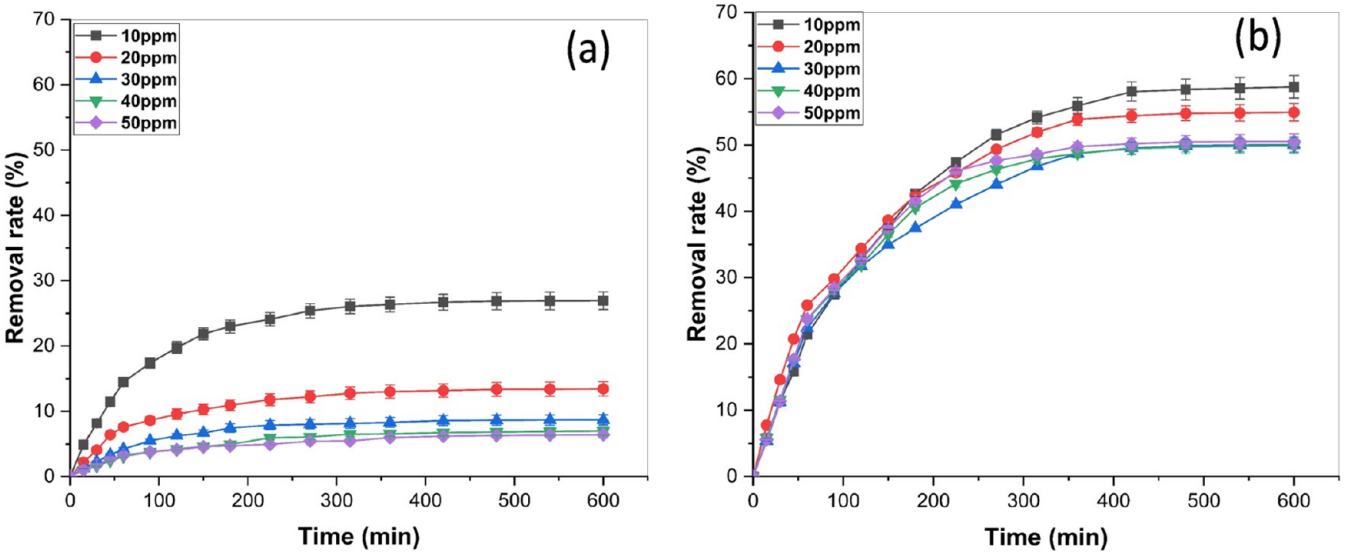

Figure 8. Effect of concentrations on the removal rate of (a) MCCH (conditions: W_{Hg} = 0.3 g, V = 30 mL, in distilled water at 298 K) and (b) Na-CMCH (conditions: W_{Hg} = 0.3 g, V = 30 mL, in distilled water at 308 K).

The cross-sectional morphology of MCCH, Na-CMCH, and after MB adsorption on the corresponding hydrogels is shown in Figure 5e−h. Figure 5e, f illustrates that the dried hydrogels had a loose and deeply porous network structure. They are suitable for the entry and adsorption of dyes and water molecules. Moreover, the swelling ability and adsorption study indicated that the hydrogels have excellent swelling and dye adsorption capability. It also can be seen in Figure 5g, h that the dye particles adsorbed onto MCCH and Na-CMCH, which can be determined clearly. The findings demonstrated that both types of hydrogels can effectively adsorb dye molecules.

4.5. EDS. The EDS spectra for MCC, MCCH, Na-CMC, and Na-CMCH are presented in Figure 6a−d. As predicted, all of the EDS spectra show significant peaks for oxygen and carbon as the primary constituents in their compositions, aligning well with the specific properties of cellulose. The percentage of carbon (C) for MCC, MCCH, Na-CMC, and Na-CMCH is 38.7, 28.2, 43.7, and 19.7%, respectively, whereas the oxygen (O) percentages for MCC, MCCH, Na-CMC, and Na-CMCH are 55.4, 33.4, 51.9, and 53.8%, respectively. In Na-CMC, the percentage of sodium (Na) is 4.3%. As we used NaOH solution in hydrogel preparation, the percentage of sodium is increased in MCCH and Na-CMCH. Sodium and chlorine were also identified in trace amounts throughout the chemical treatment operations. As NaOH, epichlorohydrin, and other chemicals were used, some small impurities appeared in the EDS spectra.

4.6. Adsorption Study. Temperature is an important parameter influencing the removal of MB by MCCH and Na-CMCH. As a result, the impact of temperature (298−318 K) on MB adsorption was also examined in this study and is presented in Figure 7. The adsorption capability improves with increasing temperature up to 308 K and then decreases dramatically. The higher diffusion rate of MB molecules within the adsorbents of Na-CMCH macropores causes the considerably increased q_e when the temperature has increased from 298 to 308 K. Because higher temperatures can help with

https://doi.org/10.1021/acsomega.3c06349
ACS Omega 2023, 8, 47856−47873

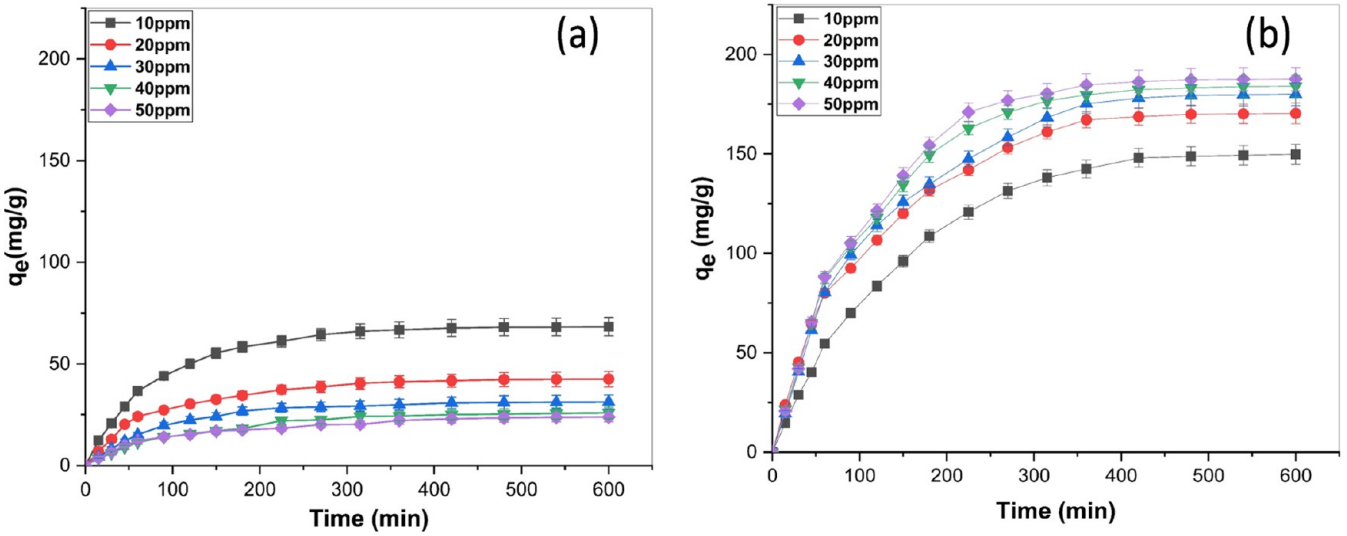

Figure 9. MB dye adsorption capacity (conditions: W_{Hg} = 0.3 g, V = 30 mL, in distilled water at 298 K) and (b) Na-CMCH (conditions: W_{Hg} = 0.3 g, V = 30 mL, in distilled water at 308 K).

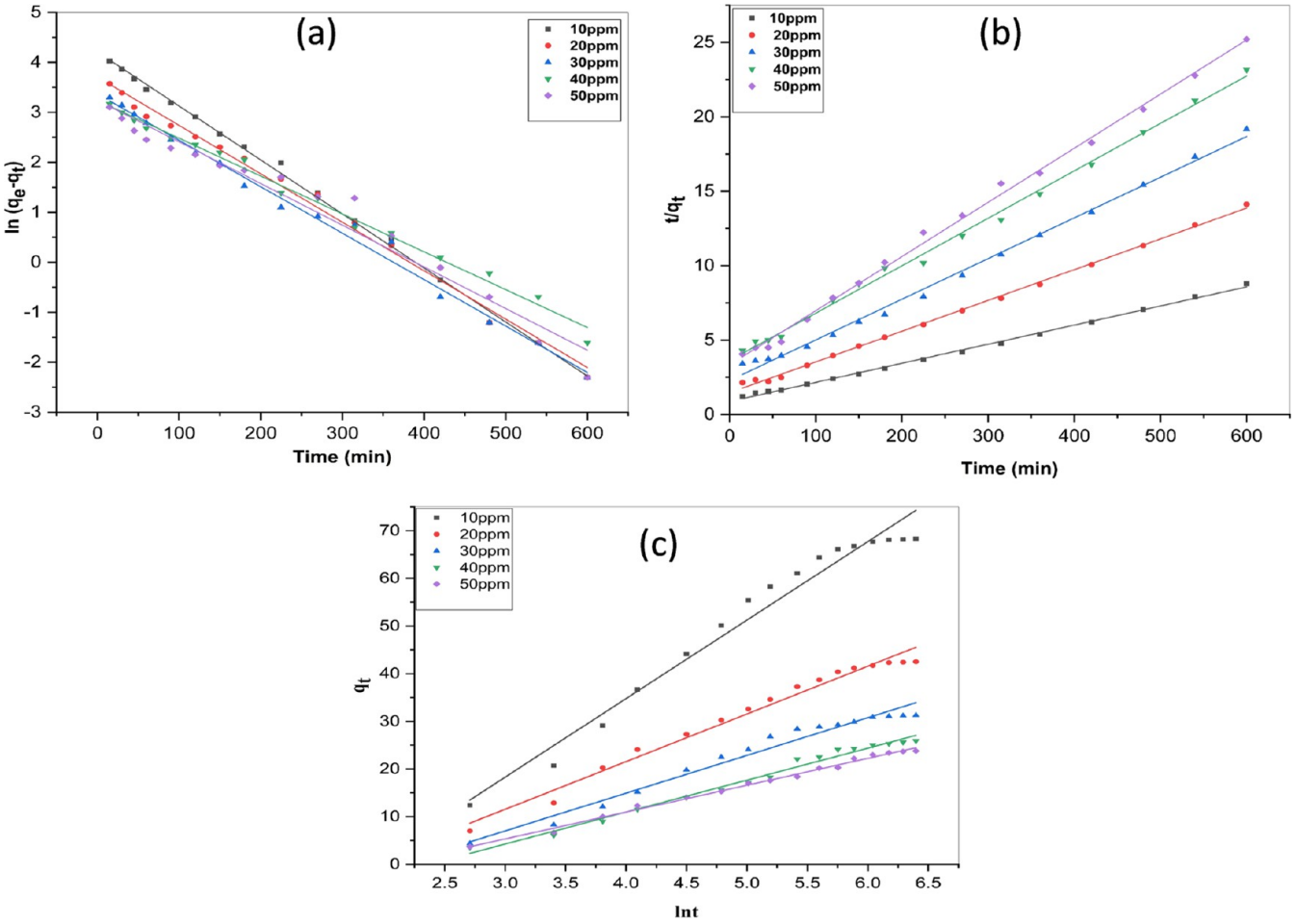

Figure 10. Linear fitting curves of kinetic plots for MCCH: (a) pseudo-first-order model, (b) pseudo-second-order, and (c) Elovich model (conditions: W_{Hg} = 0.3 g, V = 30 mL, in distilled water at 298 K).

dye adsorption and improve the mobility of large dye ions and generate a swelling impact in the interior structure, large MB molecules can pierce the adsorbent and be removed further. In contrast, increasing the temperature reduces adsorption capacity, probably because the MB molecules are so active at high temperatures that they cannot remain on the adsorbent's surface. However, the adsorption capacity for nonionic MCCH decreased with increasing temperature from 298 K.

Five MB concentrations (10, 20, 30, 40, and 50 mg/L) were chosen to evaluate the influence of the original MB

https://doi.org/10.1021/acsomega.3c06349
ACS Omega 2023, 8, 47856−47873

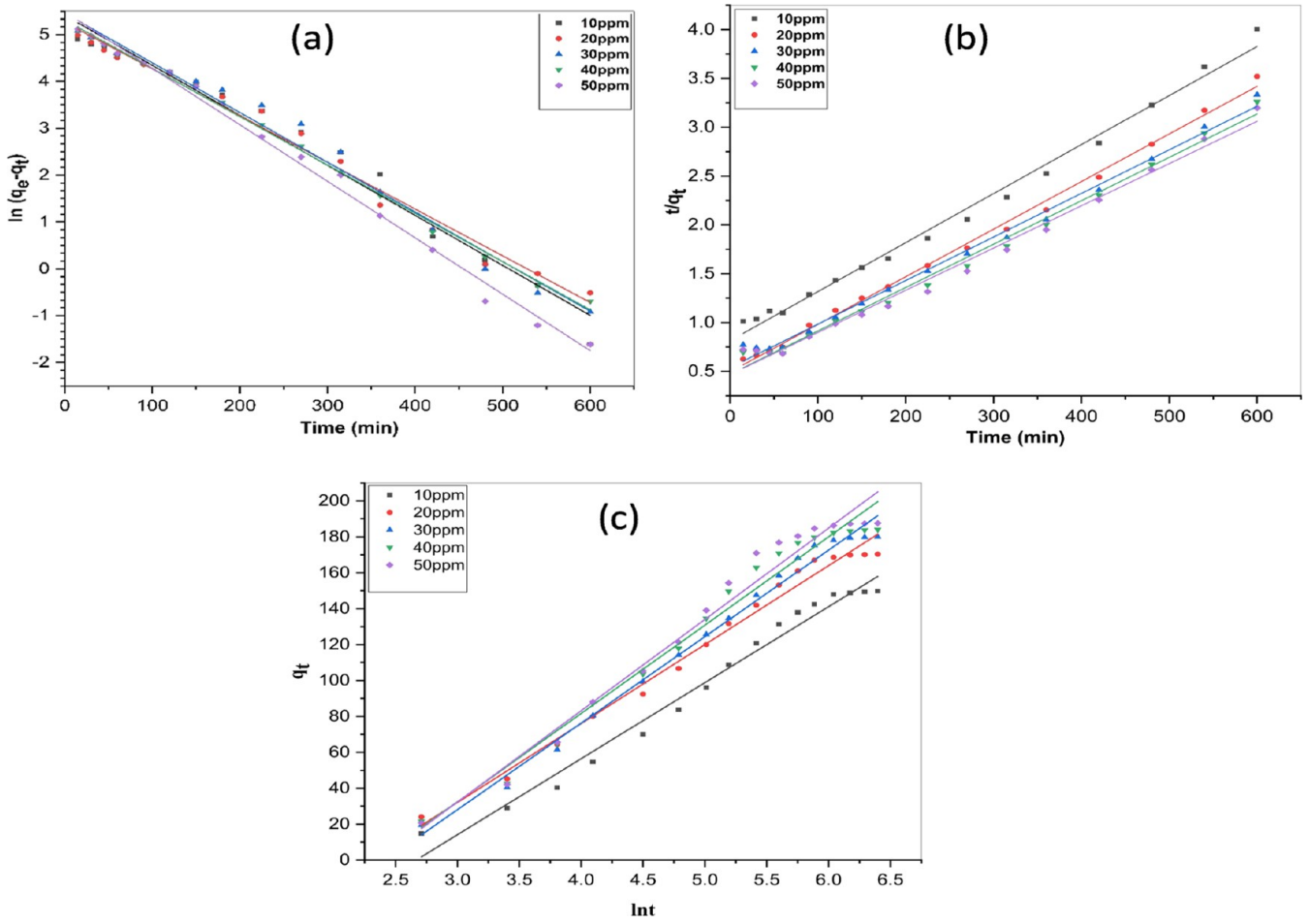

Figure 11. Linear fitting curves of kinetic plots for Na-CMCH: (a) pseudo-first-order model, (b) pseudo-second-order model, and (c) Elovich model (conditions: W_{Hg} = 0.3 g, V = 30 mL, in distilled water at 308 K).

Table 1. Parameters of the Adsorption Kinetic Process for MCCH

	model								
	pseudo-first-order			pseudo-second-order			Elovich kinetics		
conc. (mg/L)	q_e (mg/g)	K_1 (1/min) × 10^{-5}	R^2	q_e (mg/g)	k_2 (mg/min) × 10^{-4}	R^2	α (mg min/g)	β (g/mg)	R^2
10	67.26	−1.801	0.9974	77.88	1.88	0.9975	0.0607	2.4923	0.9684
20	40.77	−1.615	0.9916	48.35	2.92	0.9980	0.0999	1.5801	0.9788
30	29.07	−1.54	0.9916	36.58	3.27	0.9950	0.1262	0.9569	0.9692
40	25.53	−1.26	0.9907	31.36	2.80	0.9964	0.1491	0.6304	0.9849
50	25.64	−1.39	0.9616	27.48	3.96	0.9967	0.1774	0.6235	0.9885

concentrations on the adsorption capacity of the MCC and Na-CMC hydrogel. Figure 8 shows that the adsorption rates for both hydrogels initially rapidly increased due to the number of readily accessible active sites, and they subsequently became much slower. The percentage of dye removal effectiveness has risen as contact duration increases (up to 600 min). The maximum dye removal percentage of MCCH and Na-CMCH was found to be 26.93 ± 1.35 and 58.76 ± 1.711%, respectively. Due to the significant number of unoccupied adsorption sites, the high removal efficiency was obtained in the early stages of the adsorption period. The hydrogels are initially available for adsorption, but due to the repulsive contact between the solution phase and the MB adsorbed on the surface of the hydrogel, the remaining available surface sites became more challenging to occupy over time. Adsorption capabilities rose significantly with increasing initial low dye concentrations because of the abundance of unoccupied adsorptive sites of the adsorbent. When the original dye solution concentrations were raised further, a saturation of adsorption occurred, and there were no more accessible active sites available for adsorption. The maximal adsorption capacities for MCCH (10, 20, 30, 40, 50 mg/L) were determined to be 68.8 ± 4.245, 42.6 ± 3.789, 31.4 ± 3.451, 26.1 ± 2.845, and 23.9 ± 2.265 mg/g, and those of Na-CMCH (10, 20, 30, 40, 50 mg/L) were 150 ± 5.012, 171.01 ± 5.256, 180.4 ± 5.741, 184.5 ± 5.612, and 187.8 ± 5.841 mg/g, respectively. However, it was found that the maximum adsorption capacity of nonionic MCCH dropped when the initial concentration of MB was increased, but the maximum adsorption capacity of anionic Na-CMCH increased with increasing initial concentration of MB (Figure 9).

https://doi.org/10.1021/acsomega.3c06349
ACS Omega 2023, 8, 47856−47873

Table 2. Parameters of the Adsorption Kinetic Process for Na-CMCH

	model								
	pseudo-first-order			pseudo-second-order			Elovich kinetics		
conc. (mg/L)	q_e (mg/g)	K_1 (1/min) × 10^{-5}	R^2	q_e (mg/g)	k_2(mg/min) × 10^{-5}	R^2	α (mg min/g)	β (g/mg)	R^2
10	224.11	−1.78	0.9743	199.20	3.09	0.9906	0.02362	2.9437	0.9789
20	193.66	−1.66	0.9853	204.91	4.81	0.9965	0.02274	4.5426	0.9857
30	234.59	−1.76	0.9816	224.21	3.69	0.9927	0.02075	4.2969	0.9882
40	202.99	−1.72	0.9907	225.22	4.19	0.9908	0.02033	4.7419	0.9762
50	241.14	−2.008	0.9927	231.48	4.00	0.9968	0.01967	4.7842	0.9707

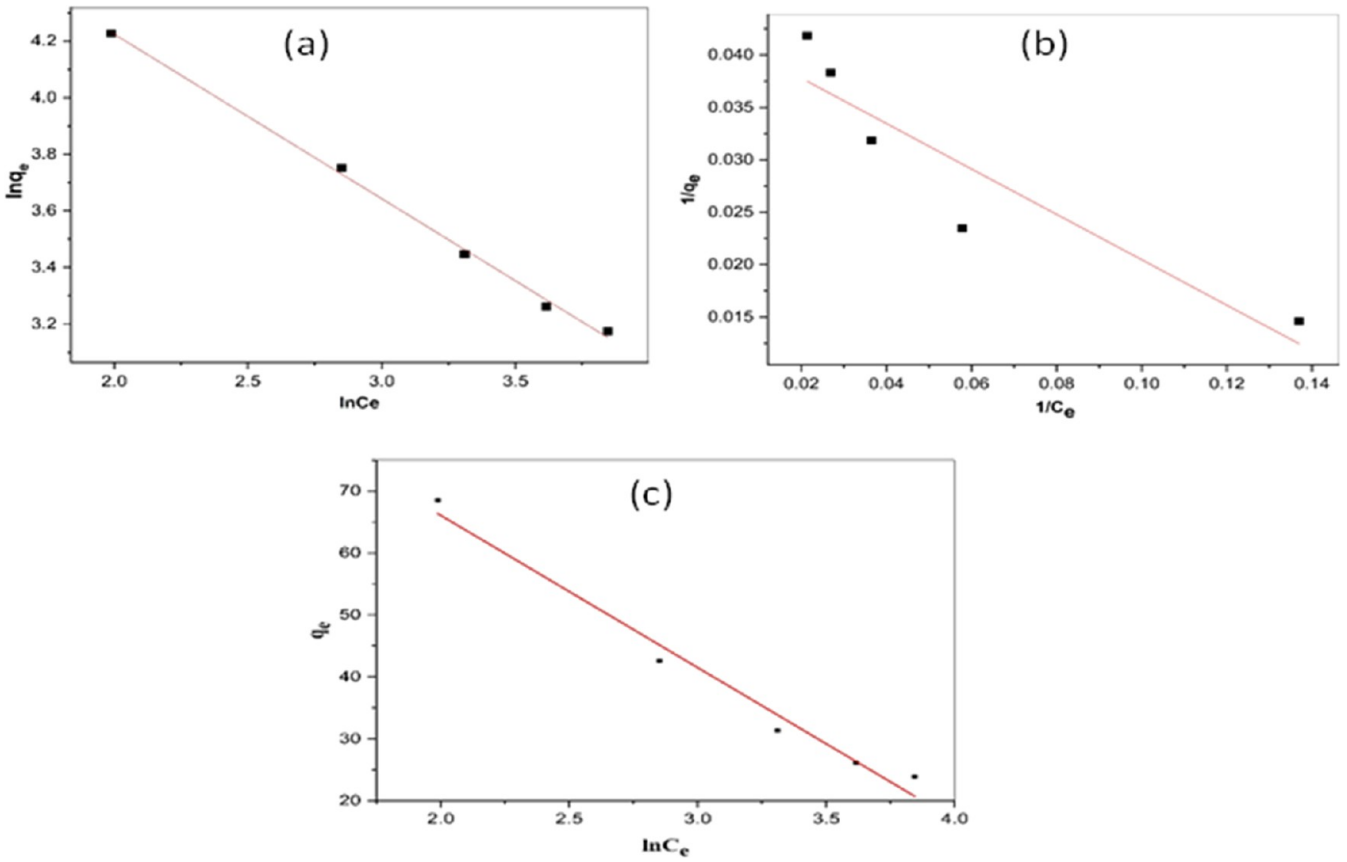

Figure 12. Fitting curves of MCCH: (a) Langmuir isotherm model, (b) Freundlich isotherm model, and (c) Temkin isotherm model (conditions: W_{Hg} = 0.3 g, V = 30 mL, in distilled water at 298 K).

4.7. Adsorption Kinetics. The adsorption kinetic behavior of MCCH and Na-CMCH was studied using the pseudo-first-order, pseudo-second-order, and Elovich models.[58] Figure 9 depicts the adsorption capacity versus time at a certain period. The adsorption rises with time until it reaches equilibrium. Figures 10 and 11 show $\log(q_e - q_t)$ graphs against time (t) for the pseudo-first-order model and t/q_t vs time for the pseudo-second-order model and q_t vs lnt for the Elovich kinetic model. Tables 1 and 2 provide the kinetic parameters and the correlation coefficient (R^2) for the adsorption process of the three kinetic models. The pseudo-second-order model is better suited for experimental data than the pseudo-first-order and Elovich models. The computed q_e values matched the experimental values, indicating a solid linear connection with an R^2 greater than 0.99.[59] Consequently, the findings demonstrated that the kinetic parameters for the adsorption process might be described using the pseudo-second-order model, and the adsorption rate depends upon both hydrogel and dye concentration.

4.8. Adsorption Isotherms. The Langmuir, Freundlich, and Temkin models (Figures 12 and 13) were utilized to investigate the interactions between the dyes and MCCH or Na-CMC hydrogels. Tables 3 and 4 provide the relevant constants and the correlation coefficient (R^2) for the Langmuir−Freundlich and Temkin models. The R^2 value of MCCH for Freundlich (R^2 = 0.9967) is larger than the values obtained for Langmuir (R^2 = 0.8563) and Temkin (R^2 = 0.9725), whereas the R^2 value of Na-CMCH for Langmuir (R^2 = 0.9974) is found to be larger than the values obtained for Freundlich (R^2 = 0.9656) and Temkin (R^2 = 0.9334). The Langmuir model assumed that adsorption takes place uniformly on the hydrogel surface and that each adsorption molecule bonded to the adsorbent surface has the same adsorption energy.[59] In contrast, the Freundlich model proposed that adsorption happens heterogeneously on the adsorbent's surface via a multilayer adsorption process, with adsorption capacity growing indefinitely with the initial concentration of the hydrogel.[60]

https://doi.org/10.1021/acsomega.3c06349
ACS Omega 2023, 8, 47856−47873

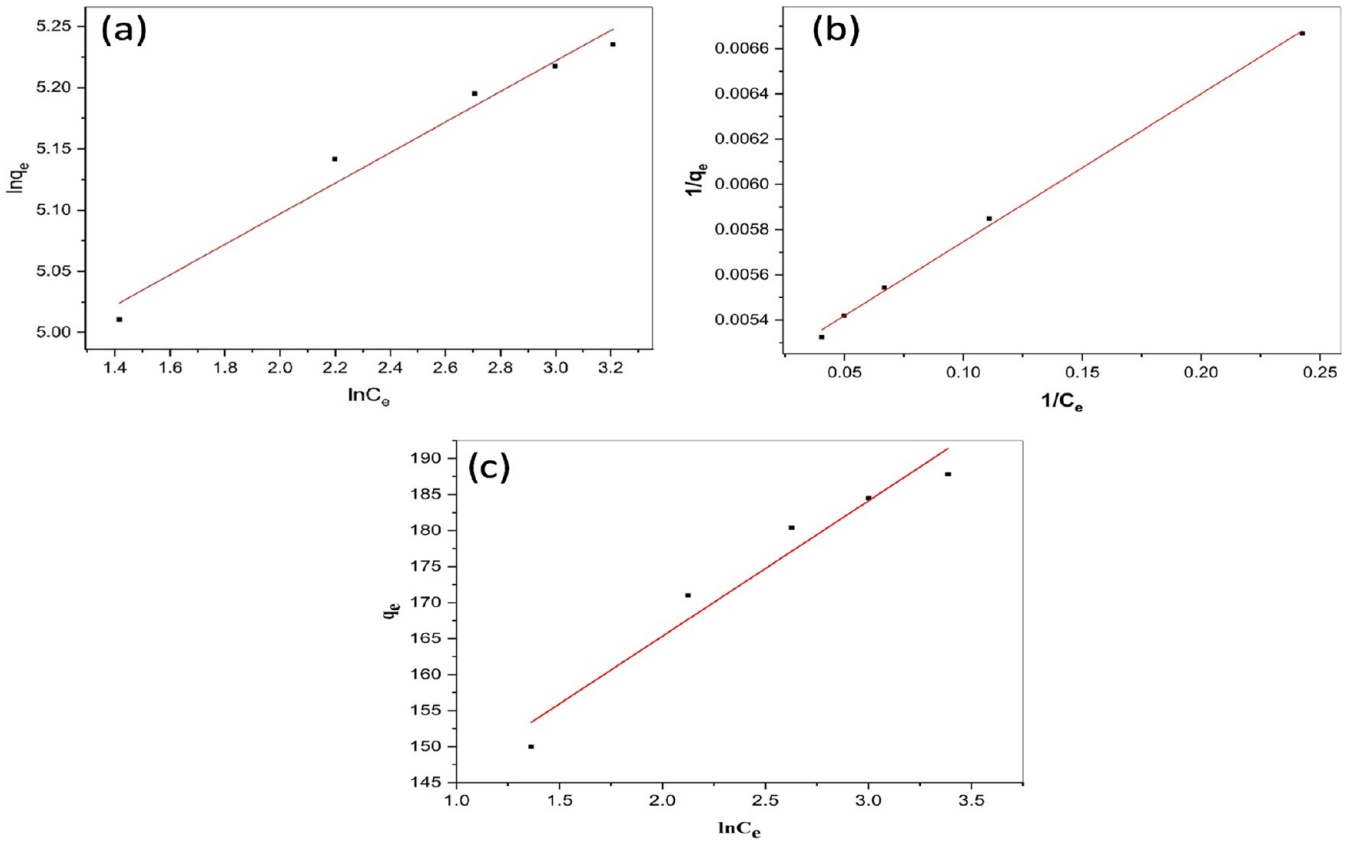

Figure 13. Fitting curves of Na-CMCH: (a) Langmuir isotherm model, (b) Freundlich isotherm model, and (c) Temkin isotherm model (conditions: W_{Hg} = 0.3 g, V = 30 mL, in distilled water at 308 K).

Table 3. Isotherm Model of Constants and Correlation Coefficients for MCCH

model									
	Langmuir isotherm			Freundlich isotherm			Temkin isotherm		
temp. (K)	q_{max} (mg/g)	K_L (L/mg)	R^2	K_F (L/mg)	n	R^2	B_T (J/mol)	K_T (L/mg)	R^2
298	23.73	−0.1945	0.8563	218.29	−1.72	0.9967	−24.58	0.0095	0.9725

Table 4. Isotherm Model of Constants and Correlation Coefficients for Na-CMCH

model									
	Langmuir isotherm			Freundlich isotherm			Temkin isotherm		
temp. (K)	q_{max} (mg/g)	K_L (L/mg)	R^2	K_F (L/mg)	n	R^2	B_T (J/mol)	K_T (L/mg)	R^2
308	196.46	0.778	0.9974	127.40	8.01	0.9656	18.78	898.01	0.9334

4.9. Adsorption Mechanism. The prominent feature of the Langmuir isotherm showed development of a single layer, indicating that saturation (a horizontal asymptote) occurs once monolayer capacity is achieved. Most theories of heterogenous catalysis and chemical adsorption are based on it. The Freundlich isotherm is an empirical equation that considers surface heterogeneity due to multilayer adsorption and the exponential distribution of adsorbent active sites and their energies toward the adsorbate.

Figures 12 and 13 showed that the fitting curve of the MCCH Freundlich model is linear. In contrast, the Na-CMCH Langmuir model is linear. This can indicate that MCCH follows the Freundlich isotherm model and Na-CMCH follows the Langmuir isotherm model. The Freundlich isotherm is the physisorption process, and Langmuir is the chemisorption process.[61] Physisorption is an exothermic process. According to Le Chatelier's principle, it decreases with increasing temperature because hydrogen bonding force acts here (shown in Scheme 3), which can be treated as weak bonding capacity. Therefore, in MCCH, with an increase in temperature, the hydrogen bonding interaction breaks down gradually. It usually takes place at low temperatures and decreases with high temperatures. At the adsorption time, MB forms a multilayer on the heterogeneous MCCH surface; as a result, the adsorption capacity is not so high. As Langmuir is chemisorption, electrostatic interactions and hydrogen bonding act in Na-CMCH, as shown in Scheme 3. Electrostatic interactions have a much stronger bonding capacity than that of hydrogen bonding.[62] As a result of both interactions, this bond has not broken down by increasing temperature but slowly at high temperatures. Therefore, the adsorption process increases with increasing temperature and decreases gradually

https://doi.org/10.1021/acsomega.3c06349
ACS Omega 2023, 8, 47856−47873

Scheme 3. Possible MB Adsorption Mechanism of MCCH and Na-CMCH

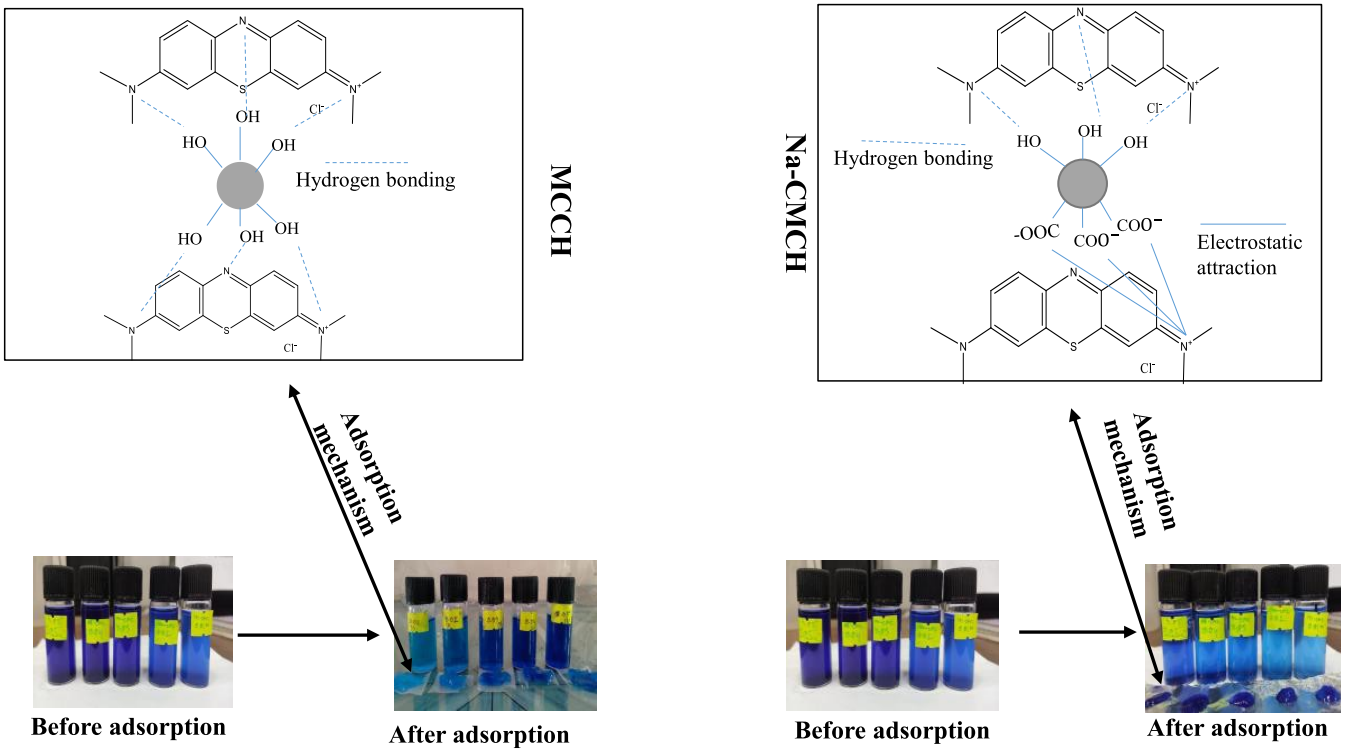

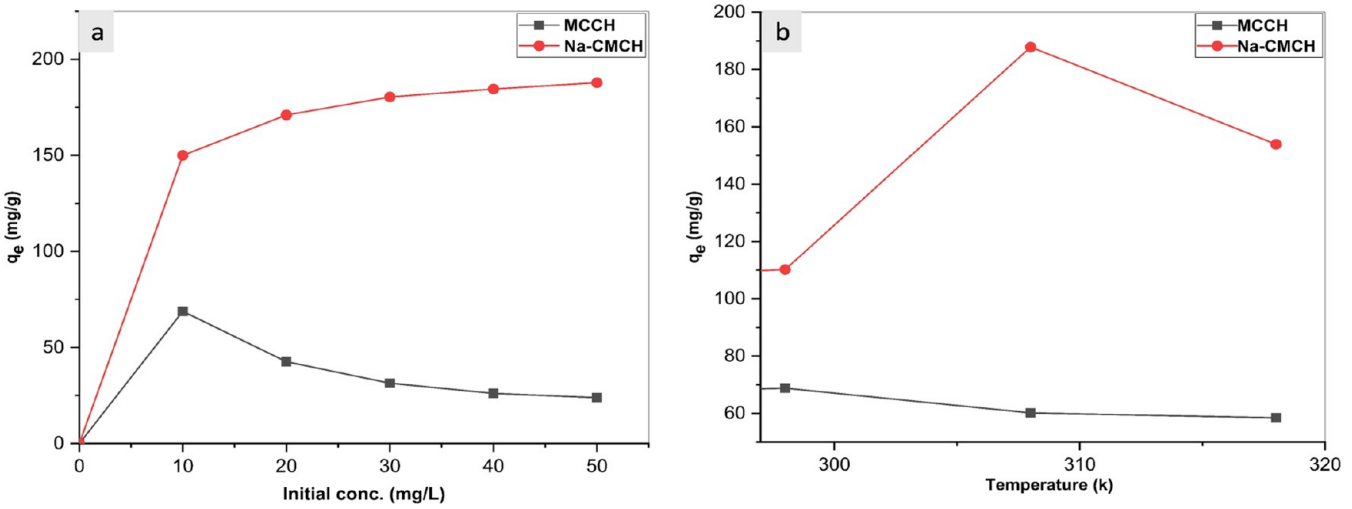

Figure 14. Difference between MCCH and Na-CMCH in various (a) initial concentrations and (b) temperatures.

in Na-CMCH. The MB forms a single layer on the homogenous surface of Na-CMCH. Consequently, the capacity of MB dye adsorption for Na-CMCH is effectively high.

4.10. Comparison between Ionic and Nonionic Hydrogels. Adsorption capacity decreases with increasing temperature and dye concentration for nonionic MCCH. It is obtained that the maximal adsorption capacity for MCCH was found to be at 298 K, whereas for Na-CMCH, it was observed to be at 308 K (Figure 14b). Adsorption capacity increases with increasing temperature and dye concentration for ionic Na-CMCH. In MCCH, the maximum adsorption capacity is obtained at 10 mg/L MB initial concentration. Still, for Na-CMCH, the concentration was reported to be 50 mg/L (Figure 14a). It could be because too many active sites exist in Na-CMCH. Relatively more vital electrostatic interactions occur between cationic MB molecules and anionic Na-CMCH hydrogels.

4.11. Reusability Study. The ability of an adsorbent to be reused several times is a crucial component in assessing the economic viability of an adsorption material. In this study, the reusability of MCCH and Na-CMCH was investigated by performing three consecutive adsorption−desorption cycles. The MB removal efficiency of both types of hydrogels decreased slightly, from 87.44 to 70.88% for MCCH and from 74.09 to 48.95% for Na-CMCH, as shown in Figure 15. The significant reduction in the removal efficiency on the adsorption−desorption process could be due to the higher swelling ability of Na-CMCH than that of the MCCH, which makes the Na-CMCH relatively unstable. Even after three

https://doi.org/10.1021/acsomega.3c06349
ACS Omega 2023, 8, 47856−47873

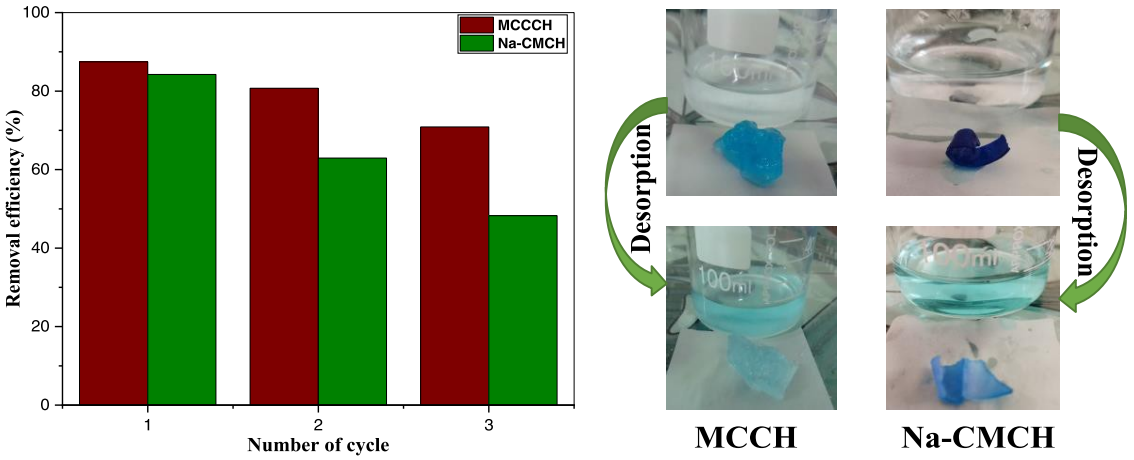

Figure 15. Removal efficiency of MB in the desorption cycle using MCCH and Na-CMCH (conditions: W_{Hg}= 0.2 g, V = 20 mL, temperature = 298 K, initial dye conc. C_o = 10 mg/L eluent = 0.1 M HCl).

cycles, the reasonably higher recycling efficiencies ensured the reuse of these hydrogels.

4.12. Treatment of Industrial Wastewater. Industrial and urban water reuse should be considered to drastically reduce total groundwater withdrawals as a future water source drastically. To realize the applicability of the synthesized hydrogel in industrial and surface water treatment, the anionic hydrogel (Na-CMCH) was explored to remove the priority heavy metal ions and organic contaminants from an industrial wastewater matrix. 0.2 g of Na-CMCH was dispersed in 20 mL of industrial wastewater after spiking with 10 mg/L MB at 25 °C for 24 h. Interestingly, it was found that Na-CMCH helps reduce the concentration of the priority toxic metal ions, and the added MB-spiked samples are also significantly reduced (Table 5). Thus, the findings suggest that Na-CMCH has great promise for cutting-edge wastewater treatment.

Table 5. MB Concentrations in Industrial Wastewater before and after Treatment with Na-CMCH at 298 K

		after treatment (μg/L)	
metal/dye	original sample (μg/L)	original sample treated with Na-CMCH	original sample spiked with MB (10,000 μg/L) and then treated with Na-CMCH
Mn	8.45	1.23	1.47
Cr	1.25	0.51	0.72
Fe	18.9	1.98	2.46
Co	1.21	0.49	0.67
Ni	1.98	0.62	0.81
Cu	6.87	2.46	2.92
Al	20.9	4.87	3.69
Pb	2.28	1.15	1.28
MB			4762

4.13. Comparative MB Adsorption Capacities of Some Previous Adsorbents. The performance of Na-CMCH and MCCH as an adsorbent to remove organic dyes (MB) from an aqueous solution in this study compared with those previously reported in the literature is presented in Table 6. It turned out that the Na-CMCH hydrogel had a distinguished position among several sorbents due to its remarkable performance. The adsorption capacity of the as-presented Na-CMCH is relatively high; the Na-CMCH hydrogel-based adsorbents can find numerous applications to treat industrial effluents in different settings.

Table 6. Comparison between Other Previous Studies and Current Adsorbents (MCCH and Na-CMCH)

types of adsorbents	adsorbates	q_{max} (mg/g)	ref.
Na-CMCH	MB	194.46	this study
MCCH	MB	23.73	this study
Gum-arabic/poly(AA-*co*-AM)	MB	269.2	63
P(AAm-*co*-MEA)	MB	48	64
Poly(AA-*co*-AM-*co*-SH)	MB	39.5	65
GH hydrogels	MB	60.32	59
mwXG-gPAA	MB	149.25	3

5. CONCLUSIONS

This research shows that jute sticks may be used as an alternative to MCC isolation. Na-CMC was successfully synthesized from the isolated MCC. MCCH and Na-CMCH were prepared using epichlorohydrin (ECH) in excellent yields by a chemical crosslinking method. Isolated MCC, synthesized Na-CMC, and the corresponding hydrogels were characterized by FTIR, XRD, SEM, and EDS for functional groups, crystallinity, surface morphology, and elemental composition determination, respectively. Both types of hydrogels were used to remove MB from the aqueous solution at different contact times (up to 600 min), initial MB concentrations (10−50 mg/L), and temperatures (298−318 K). The removal percentage of MB by Na-CMCH and MCCH under the optimum conditions was 58.73 and 26.93%, respectively (C_o = 10 mg/L, W_{Hg} = 0.3 g, V = 30 mL, T = 298 K (MCCH) and T= 308 K (Na-CMCH)). Na-CMCH has shown a higher adsorption capacity (194.46 mg/g) than that of MCCH (23.73 mg/g) between the two adsorbents. The adsorption capacity of MCCH decreases with increasing initial dye concentration (10−50 mg/L) and temperature (298−318 K), but at the same conditions, the adsorption capacity of Na-CMCH increases. MCCH follows the Freundlich model (R^2 = 0.9967), and Na-CMCH follows the Langmuir isotherm model (R^2 = 0.9974). The pseudo-second-order kinetic model is favorable for both hydrogels. The adsorption/desorption efficiencies of the hydrogels were found to be reasonably high, indicating their reusability and recyclability. Both the spiked industrial wastewater and aqueous solution

https://doi.org/10.1021/acsomega.3c06349
ACS Omega 2023, 8, 47856−47873

had the MB effectively removed by Na-CMCH. Additionally, Na-CMCH significantly decreased the priority metal ions in an industrial effluent. Overall, the results showed that the studied adsorbents have great potential for industrial application to remove dyes from industrial wastewater. Moreover, agricultural waste (jute sticks) was converted into a valuable commodity as a cellulose-based hydrogel material, which can be used as an adsorbent to remove dyes from aqueous solutions.

AUTHOR INFORMATION

Corresponding Author

Md. Maniruzzaman − *Department of Chemistry, Khulna University of Engineering & Technology, Khulna 9203, Bangladesh;* orcid.org/0000-0001-8678-4659; Email: mzaman_103@chem.kuet.ac.bd

Authors

Md. Sabbir Ahmed − *Department of Chemistry, Khulna University of Engineering & Technology, Khulna 9203, Bangladesh*

Md. Rubel Al-Mamun − *Department of Chemistry, Khulna University of Engineering & Technology, Khulna 9203, Bangladesh*

Mohammad Amdad Ali − *Illinois Materials Research Laboratory, University of Illinois at Urbana-Champaign, Urbana, Illinois 61801, United States*

Md. Mizanur Rahman Badal − *Department of Chemistry, Khulna University of Engineering & Technology, Khulna 9203, Bangladesh;* orcid.org/0000-0002-4119-4337

Md. Abdul Aziz − *Interdisciplinary Research Center for Hydrogen and Energy Storage (IRC-HES), King Fahd University of Petroleum and Minerals, Dhahran 31261, Saudi Arabia;* orcid.org/0000-0002-1537-2785

Mohammad A. Jafar Mazumder − *Department of Chemistry and Interdisciplinary Research Center for Advanced Materials, King Fahd University of Petroleum & Minerals, Dhahran 31261, Saudi Arabia*

Abbas Saeed Hakeem − *Interdisciplinary Research Center for Hydrogen and Energy Storage (IRC-HES), King Fahd University of Petroleum and Minerals, Dhahran 31261, Saudi Arabia*

Mohammad Abu Yousuf − *Department of Chemistry, Khulna University of Engineering & Technology, Khulna 9203, Bangladesh*

Complete contact information is available at: https://pubs.acs.org/10.1021/acsomega.3c06349

Notes

The authors declare no competing financial interest.

ACKNOWLEDGMENTS

The authors would like to thank the Khulna University of Engineering & Technology for financial support and necessary facilities. The authors are also grateful to the Department of Chemistry for providing the required facilities for conducting this research.

REFERENCES

(1) Shirzad-Siboni, M.; Jafari, S. J.; Giahi, O.; Kim, I.; Lee, S. M.; Yang, J. K. Removal of acid blue 113 and reactive black 5 dye from aqueous solutions by activated red mud. *J. Ind. Eng. Chem.* **2014**, *20* (4), 1432−1437.

(2) Monsef, R.; Ghiyasiyan-Arani, M.; Amiri, O.; Salavati-Niasari, M. Sonochemical synthesis, characterization and application of PrVO4 nanostructures as an effective photocatalyst for discoloration of organic dye contaminants in wastewater. *Ultrason. Sonochem.* **2020**, *61*, No. 104822.

(3) Makhado, E.; Pandey, S.; Nomngongo, P. N.; Ramontja, J. Fast microwave-assisted green synthesis of xanthan gum grafted acrylic acid for enhanced methylene blue dye removal from aqueous solution. *Carbohydr. Polym.* **2017**, *176*, 315−326.

(4) Dang, X.; Yu, Z.; Yang, M.; Woo, M. W.; Song, Y.; Wang, X.; Zhang, H. Sustainable electrochemical synthesis of natural starch-based biomass adsorbent with ultrahigh adsorption capacity for Cr (VI) and dyes removal. *Sep. Purif. Technol.* **2022**, *288*, No. 120668.

(5) Saravanan, S.; Sivasankar, T. Effect of ultrasound power and calcination temperature on the sonochemical synthesis of copper oxide nanoparticles for textile dyes treatment. *Environ. Prog. Sustainable Energy* **2016**, *35* (3), 669−679.

(6) Ghaderi, A.; Abbasi, S.; Farahbod, F. Synthesis of SnO2 and ZnO nanoparticles and SnO2-ZnO hybrid for the photocatalytic oxidation of methyl orange. *Iran. J. Chem. Eng.* **2015**, *12* (3), 96−105.

(7) Shayesteh, H.; Raji, F.; Kelishami, A. R. Influence of the alkyl chain length of surfactant on adsorption process: a case study. *Surf. Interfaces* **2021**, *22*, No. 100806.

(8) Ali, S. A.; Mubarak, S. A.; Yaagoob, I. Y.; Arshad, Z.; Mazumder, M. A. A sorbent containing pH-responsive chelating residues of aspartic and maleic acids for mitigation of toxic metal ions, cationic, and anionic dyes. *RSC Adv.* **2022**, *12* (10), 5938−5952.

(9) Koochakzadeh, F.; Norouzbeigi, R.; Shayesteh, H. Statistically optimized sequential hydrothermal route for FeTiO3 surface modification: Evaluation of hazardous cationic dyes adsorptive removal. *Environ. Sci. Pollut. Res.* **2023**, *30* (7), 19167−19181.

(10) Sun, J.; Sun, G.; Zhao, X.; Liu, X.; Zhao, H.; Xu, C.; Yan, L.; Jiang, X.; Cui, Y. Ultrafast and efficient removal of Pb (II) from acidic aqueous solution using a novel polyvinyl alcohol superabsorbent. *Chemosphere* **2021**, *282*, No. 131032.

(11) Masry, B. A.; Elhady, M. A.; Mousaa, I. M. Fabrication of a novel polyvinylpyrrolidone/abietic acid hydrogel by gamma irradiation for the recovery of Zn, Co, Mn and Ni from aqueous acidic solution. *Inorg. Nano-Met. Chem.* **2023**, *53* (3), 283−294.

(12) Mazumder, M. A. J. Polymeric Adsorbents: Innovative Materials for Water Treatments. *Curr. Anal. Chem.* **2023**, *19* (2), 105−110.

(13) Ali, S. A.; Arshad, Z.; Goni, L. K.; Yaagoob, I. Y.; Al-Muallem, H. A.; Mazumder, M. A. Cross-linked cyclopolymers from pH-Responsive diallyl amine salts for environmental remediation. *J. Environ. Chem. Eng.* **2023**, *11*, No. 110995.

(14) Huber, T.; Müssig, J.; Curnow, O.; Pang, S.; Bickerton, S.; Staiger, M. P. A critical review of all-cellulose composites. *J. Mater. Sci.* **2012**, *47*, 1171−1186.

(15) Trache, D.; Khimeche, K.; Mezroua, A.; Benziane, M. Physicochemical properties of microcrystalline nitrocellulose from Alfa grass fibers and its thermal stability. *J. Therm. Anal. Calorim.* **2016**, *124* (3), 1485−1496.

(16) Nayak, R.; Houshyar, S.; Khandual, A.; Padhye, R.; Fergusson, S. Identification of Natural Textile Fibres. In *Handbook of Natural Fibres*; Woodhead Publishing, 2020; pp 503−534.

(17) Nwachukwu, N.; Ugoeze, K. C. Studies on Microcrystalline Cellulose Obtained From Saccharum Officinarum 2: Flow and Compaction Properties. *J. Drug Delivery Ther.* **2018**, *8* (2), 54−59.

(18) Rivai, H.; Hamdani, A. S.; Ramdani, R.; Lalfari, R. S.; Andayani, R.; Armin, F.; Djamaan, A. Production and characterization of alpha cellulose derived from rice straw (Oryza sativa L.). *Int. J. Pharm. Sci. Rev. Res.* **2018**, *52*, 45−48.

(19) Wu, H.; Chen, F.; Liu, M.; Wang, J. Preparation of microcrystalline cellulose by liquefaction of eucalyptus sawdust in ethylene glycol catalyzed by acidic ionic liquid. *BioResources* **2017**, *12* (2), 3766−3777.

(20) Nasatto, P. L.; Pignon, F.; Silveira, J. L.; Duarte, M. E. R.; Noseda, M. D.; Rinaudo, M. Methylcellulose, a cellulose derivative

https://doi.org/10.1021/acsomega.3c06349
ACS Omega 2023, 8, 47856−47873

with original physical properties and extended applications. *Polymers* **2015**, *7* (5), 777−803.
(21) Izzati Zulkifli, N.; Samat, N.; Anuar, H.; Zainuddin, N. Mechanical properties and failure modes of recycled polypropylene/microcrystalline cellulose composites. *Mater. Des.* **2015**, *69*, 114−123.
(22) Sun, X.; Lu, C.; Liu, Y.; Zhang, W.; Zhang, X. Melt-processed poly (vinyl alcohol) composites filled with microcrystalline cellulose from waste cotton fabrics. *Carbohydr. Polym.* **2014**, *101*, 642−649.
(23) Haafiz, M. M.; Hassan, A.; Zakaria, Z.; Inuwa, I. M.; Islam, M. S.; Jawaid, M. Properties of polylactic acid composites reinforced with oil palm biomass microcrystalline cellulose. *Carbohydr. Polym.* **2013**, *98* (1), 139−145.
(24) Rineksa, G.; Whulanza, Y.; Gozan, M. Preliminary Study of Potential Bioimplant from Glycerol Plasticized Starch-Microcrystalline Cellulose Composite. *J. Integr. Adv. Eng.* **2021**, *1* (1), 29−36.
(25) Lu, H.; Sun, S.; Sun, J.; Peng, X.; Li, N.; Ullah, M. W.; Zhang, Y.; Chen, L.; Zhou, J. Sustainable production of flocculant-containing bacterial cellulose composite for removal of PET nano-plastics. *Chem. Eng. J.* **2023**, *469*, No. 143848.
(26) Setu, M. N. I.; Mia, M. Y.; Lubna, N. J.; Chowdhury, A. A. Preparation of microcrystalline cellulose from cotton and its evaluation as direct compressible excipient in the formulation of Naproxen tablets. *Dhaka Univ. J. Pharm. Sci.* **2015**, *13* (2), 187−192.
(27) Bhandari, K.; Roy, P.; Bhattacharyya, A. R.; Maulik, S. R. Synthesis and characterization of microcrystalline cellulose from jute stick. *Indian J. Fibre Text. Res.* **2021**, *45* (4), 464−469.
(28) Agustin-Salazar, S.; Cerruti, P.; Medina-Juárez, L.Á.; Scarinzi, G.; Malinconico, M.; Soto-Valdez, H.; Gamez-Meza, N. Lignin and holocellulose from pecan nutshell as reinforcing fillers in poly (lactic acid) biocomposites. *Int. J. Biol. Macromol.* **2018**, *115*, 727−736.
(29) Espinosa, E.; Sánchez, R.; Otero, R.; Domínguez-Robles, J.; Rodríguez, A. A comparative study of the suitability of different cereal straws for lignocellulose nanofibers isolation. *Int. J. Biol. Macromol.* **2017**, *103*, 990−999.
(30) Ren, W.; Guo, F.; Zhu, J.; Cao, M.; Wang, H.; Yu, Y. A comparative study on the crystalline structure of cellulose isolated from bamboo fibers and parenchyma cells. *Cellulose* **2021**, *28* (10), 5993−6005.
(31) Kunusa, W. R.; Isa, I.; Laliyo, L. A.; Iyabu, H. FTIR, XRD and SEM Analysis of Microcrystalline Cellulose (MCC) Fibers from Corncorbs in Alkaline Treatment. In *Journal of Physics: Conference Series*; IOP Publishing, 2018; Vol. *1028*, 012199.
(32) Hassan, M. L.; Berglund, L.; Abou Elseoud, W. S.; Hassan, E. A.; Oksman, K. Effect of pectin extraction method on properties of cellulose nanofibers isolated from sugar beet pulp. *Cellulose* **2021**, *28*, 10905−10920.
(33) Adewuyi, A.; Pereira, F. V. Isolation and surface modification of cellulose from underutilized Luffa cylindrica sponge: A potential feed stock for local polymer industry in Africa. *J. Assoc. Arab Univ. Basic Appl. Sci.* **2017**, *24* (1), 39−45.
(34) Hasanin, M. S.; Kassem, N.; Hassan, M. L. Preparation and characterization of microcrystalline cellulose from olive stones. *Biomass Convers. Biorefin.* **2021**, 1−8.
(35) Dhali, K.; Daver, F.; Cass, P.; Adhikari, B. Isolation and characterization of cellulose nanomaterials from jute bast fibers. *J. Environ. Chem. Eng.* **2021**, *9* (6), No. 106447.
(36) Gorade, V. G.; Kotwal, A.; Chaudhary, B. U.; Kale, R. D. Surface modification of microcrystalline cellulose using rice bran oil: A bio-based approach to achieve water repellency. *J. Polym. Res.* **2019**, *26*, 1−12.
(37) Gong, R.; Ma, Z.; Wang, X.; Han, Y.; Guo, Y.; Sun, G.; Li, Y.; Zhou, J. Sulfonic-acid-functionalized carbon fiber from waste newspaper as a recyclable carbon based solid acid catalyst for the hydrolysis of cellulose. *RSC Adv.* **2019**, *9* (50), 28902−28907.
(38) Li, M.; He, B.; Zhao, L. Isolation and characterization of microcrystalline cellulose from Cotton Stalk Waste. *BioResources* **2019**, *14* (2), 3231−3246.
(39) Mohamad Haafiz, M.; Eichhorn, S. J.; Hassan, A.; Jawaid, M. Isolation and characterization of microcrystalline cellulose from oil palm biomass residue. *Carbohydr. Polym.* **2013**, *93* (2), 628−634.
(40) Obumneme O, O. The effect of pulping concentration treatment on the properties of microcrystalline cellulose powder obtained from waste paper. *Carbohydr. Polym.* **2013**, *98* (1), 721−725.
(41) Merci, A.; Urbano, A.; Grossmann, M. V. E.; Tischer, C. A.; Mali, S. Properties of microcrystalline cellulose extracted from soybean hulls by reactive extrusion. *Food Res. Int.* **2015**, *73*, 38−43.
(42) Ahmadi, M.; Madadlou, A.; Sabouri, A. A. Isolation of micro- and nano-crystalline cellulose particles and fabrication of crystalline particles-loaded whey protein cold-set gel. *Food Chem.* **2015**, *174*, 97−103.
(43) Chaiwutthinan, P.; Pimpan, V.; Chuayjuljit, S.; Leejarkpai, T. Biodegradable plastics prepared from poly (lactic acid), poly (butylene succinate) and microcrystalline cellulose extracted from waste-cotton fabric with a chain extender. *J. Polym. Environ.* **2015**, *23*, 114−125.
(44) Gon, D.; Das, K.; Paul, P.; Maity, S. Jute composites as wood substitute. *Int. J. Text. Sci.* **2012**, *1* (6), 84−93.
(45) Nayak, L.; Ray, D. P.; Shambhu, V. B. Appropriate technologies for conversion of jute biomass into energy. *Int. J. Emerg. Technol. Adv. Eng.* **2013**, *3*, 570−574.
(46) Matin, M.; Rahaman, M. M.; Nayeem, J.; Sarkar, M.; Jahan, M. S. Dissolving pulp from jute stick. *Carbohydr. Polym.* **2015**, *115*, 44−48.
(47) Jerman, A.; Bertoncelj, A.; Dominici, G.; Bach, M. P.; Trnavčević, A. Conceptual key competency model for smart factories in production processes. *Organizacija* **2020**, *53* (1), 68−79.
(48) Wu, Z.; Cheng, Z.; Ma, W. Adsorption of Pb (II) from glucose solution on thiol-functionalized cellulosic biomass. *Bioresour. Technol.* **2012**, *104*, 807−809.
(49) Zhang, M.; Yang, M.; Woo, M. W.; Li, Y.; Han, W.; Dang, X. High-mechanical strength carboxymethyl chitosan-based hydrogel film for antibacterial wound dressing. *Carbohydr. Polym.* **2021**, *256*, No. 117590.
(50) Suryadi, H.; Sari, H. R.; et al. Preparation of microcrystalline cellulose from water hyacinth powder by enzymatic hydrolysis using cellulase of local isolate. *J. Young Pharm.* **2017**, *9* (1s), S19.
(51) Hong, K. M. *Preparation and Characterization of Carboxymethyl Cellulose From Sugarcane Bagasse.[Skripsi]*; Universiti Tunku Abdul Rahman: Malaysia, 2013.
(52) Qin, X.; Lu, A.; Zhang, L. Gelation behavior of cellulose in NaOH/urea aqueous system via cross-linking. *Cellulose* **2013**, *20*, 1669−1677.
(53) Yadollahi, M.; Gholamali, I.; Namazi, H.; Aghazadeh, M. Synthesis and characterization of antibacterial carboxymethyl cellulose/ZnO nanocomposite hydrogels. *Int. J. Biol. Macromol.* **2015**, *74*, 136−141.
(54) Nguyen, M. N.; Tran, T. T.; Nguyen, Q. T.; Tran Thi, T.; Nguyen, B. C.; Hollmann, D. Simple synthesis of cellulose hydrogels based on the direct dissolution of cellulose in tetrabutylphosphonium hydroxide followed by cross-linking. *Polym. Adv. Technol.* **2022**, *33* (10), 3376−3385.
(55) Suripto, S.; Noviany, N.; Wasinton, S.; Kiswandono, A. A.; Sutopo, H. *Similarity Characterization of Carboxymethyl Cellulose (CMC) Synthesized from Microcellulose of Cassava Peel*, 2021.
(56) Hoogendam, C. W.; de Keizer, A.; Cohen Stuart, M. A.; Bijsterbosch, B. H.; Smit, J. A. M.; van Dijk, J. A. P. P.; van der Horst, P. M.; Batellaan, J. G. Persistence length of carboxymethyl cellulose as evaluated from size exclusion chromatography and potentiometric titrations. *Macromolecules* **1998**, *31*, 6297−6309.
(57) Hu, X.-S.; Liang, R.; Sun, G. Superadsorbent hydrogel for removal of methylene blue dye from aqueous solution. *J. Mater. Chem. A* **2018**, *6* (36), 1−18.
(58) Shayesteh, H.; Ashrafi, A.; Rahbar-Kelishami, A. Evaluation of Fe_3O_4@ MnO_2 core-shell magnetic nanoparticles as an adsorbent for decolorization of methylene blue dye in contaminated water:

https://doi.org/10.1021/acsomega.3c06349
ACS Omega 2023, 8, 47856−47873

Synthesis and characterization, kinetic, equilibrium, and thermodynamic studies. *J. Mol. Struct.* **2017**, *1149*, 199−205.
(59) Ren, J.; Wang, X.; Zhao, L.; Li, M.; Yang, W. Effective removal of dyes from aqueous solutions by a gelatin hydrogel. *J. Polym. Environ.* **2021**, *29*, 1−12.
(60) Sharma, G.; Kumar, A.; Naushad, M.; García-Peñas, A.; Ala'a, H.; Ghfar, A. A.; Sharma, V.; Ahamad, T.; Stadler, F. J. Fabrication and characterization of Gum arabic-cl-poly (acrylamide) nanohydrogel for effective adsorption of crystal violet dye. *Carbohydr. Polym.* **2018**, *202*, 444−453.
(61) Zaheer, Z.; Bawazir, W. A.; Al-Bukhari, S. M.; Basaleh, A. S. Adsorption, equilibrium isotherm, and thermodynamic studies to the removal of acid orange 7. *Mater. Chem. Phys.* **2019**, *232*, 109−120.
(62) Weinhold, F.; Klein, R. A. Anti-electrostatic hydrogen bonds. *Angew. Chem., Int. Ed.* **2014**, *53* (42), 11214−11217.
(63) Singh, T.; Singhal, R. Poly (acrylic acid/acrylamide/sodium humate) superabsorbent hydrogels for metal ion/dye adsorption: Effect of sodium humate concentration. *J. Appl. Polym. Sci.* **2012**, *125* (2), 1267−1283.
(64) Paulino, A. T.; Guilherme, M. R.; Reis, A. V.; Campese, G. M.; Muniz, E. C.; Nozaki, J. Removal of methylene blue dye from an aqueous media using superabsorbent hydrogel supported on modified polysaccharide. *J. Colloid Interface Sci.* **2006**, *301* (1), 55−62.
(65) Işikver, Y. Removal of some cationic dyes from aqueous solution by acrylamide-or 2-hydroxyethyl methacrylate-based copolymeric hydrogels. *Fibers Polym.* **2017**, *18*, 2070−2078.

https://doi.org/10.1021/acsomega.3c06349
ACS Omega 2023, 8, 47856−47873